

# PRERESQ-R1: TOWARDS FINE-GRAINED RANK-AND-SCORE REINFORCEMENT LEARNING FOR VISUAL QUALITY ASSESSMENT VIA PREFERENCE-RESPONSE DISENTANGLED POLICY OPTIMIZATION

Zehui Feng<sup>1</sup>, Tian Qiu<sup>1</sup>, Tong Wu<sup>1</sup>, Junxuan Li<sup>1</sup>, Huayuan Xu<sup>1</sup>, Ting Han<sup>1,2</sup> \*

<sup>1</sup>Shanghai Jiao Tong University, Shanghai, China

<sup>2</sup>Zhejiang University, Hangzhou, China

{fzh\_sjtu, autumn0918, mumumumu, xuan136, hwawon, hanting}@sjtu.edu.cn

<https://github.com/DanceSkyCode/General-Visual-Quality-RL>

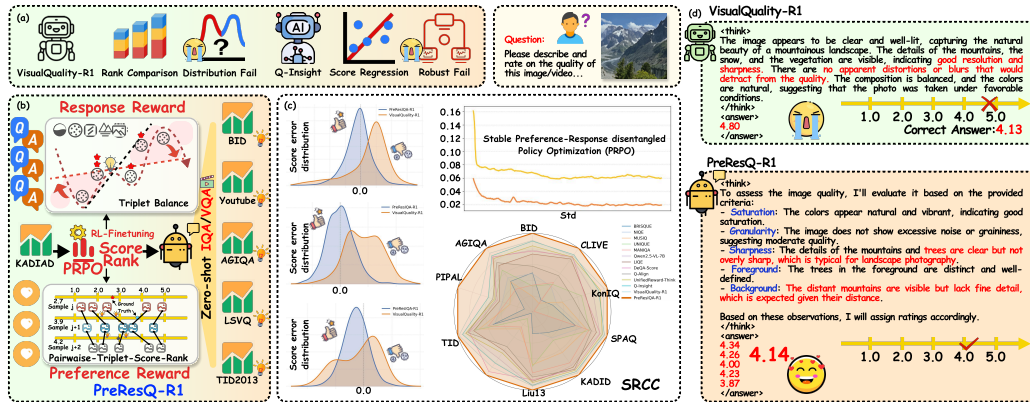


Figure 1: **Overview Performance.** (a) Existing score/ranking reward function assign minimal difference, which results in distribution fall or robustness fail. (b) PreResQ-R1 focus on fine-grained response-ranking reward balance and preference. (c) PreResQ-R1 enables state-of-the-art performance and stable image quality assessment with discriminative reward. (d) typical qualitative and quantitative example comparison between VisualQuality-R1 and PreResQ-R1, which demonstrates superior performance on image quality describe and score.

## ABSTRACT

Visual Quality Assessment (QA) seeks to predict human perceptual judgments of visual fidelity. While recent multimodal large language models (MLLMs) show promise in reasoning about image and video quality, existing approaches mainly rely on supervised fine-tuning or rank-only objectives, resulting in shallow reasoning, poor score calibration, and limited cross-domain generalization. We propose PreResQ-R1, a Preference-Response Disentangled Reinforcement Learning framework that unifies absolute score regression and relative ranking consistency within a single reasoning-driven optimization scheme. Unlike prior QA methods, PreResQ-R1 introduces a dual-branch reward formulation that separately models intra-sample response coherence and inter-sample preference alignment, optimized via Group Relative Policy Optimization (GRPO). This design encourages fine-grained, stable, and interpretable chain-of-thought reasoning about perceptual quality. To extend beyond static imagery, we further design a global-temporal and local-spatial data flow strategy for Video Quality Assessment. Remarkably, with reinforcement fine-tuning on only 6K images and 28K videos, PreResQ-R1 achieves state-of-the-art results across 10 IQA and 5 VQA benchmarks under both SRCC and PLCC metrics, surpassing by margins of **5.30%** and **2.15%** in IQA task, respectively. Beyond quantitative gains, it produces human-aligned reasoning traces that reveal the perceptual cues underlying quality judgments. Code and model are available.

\*Corresponding authors.

## 1 INTRODUCTION

Visual Quality Assessment (QA) aims to predict human perceptual judgments of visual fidelity and serves as a fundamental capability in computer vision applications such as image enhancement Chen et al. (2024); Zheng et al. (2021), generation Yu et al. (2024b); Chen et al. (2025b), and computational photography Cai et al. (2024). Depending on reference availability, QA methods are categorized into full-reference (FR) and no-reference (NR) approaches Wang et al. (2004), with the latter being particularly challenging and practical when pristine references are absent. Early NR-QA models based on handcrafted natural scene statistics Mittal et al. (2012) struggled to generalize across complex distortions. Deep learning-based regressors Ke et al. (2021); You et al. (2025) improved prediction accuracy but often overfit to specific datasets, resulting in unstable generalization. Ranking-based methods Ying et al. (2019); Liu et al. (2017) alleviate this by modeling relative perceptual orderings, yet they neglect fine-grained score calibration, reducing interpretability and robustness. The core challenge remains how to unify absolute scoring and relative ranking within an interpretable framework.

Recent advances in multimodal large language models (MLLMs) Touvron et al. (2023); Bai et al. (2025) demonstrate strong reasoning and generalization through chain-of-thought (CoT) mechanisms Wang et al. (2025a), linking low-level distortions with high-level semantics Li et al. (2025); Wu et al. (2023c). However, existing MLLM-based QA systems largely rely on supervised fine-tuning, suffering from costly annotation, overfitting to dataset-specific score distributions, and shallow reasoning due to the absence of explicit CoT optimization. Reinforcement learning (RL) offers a promising alternative for aligning models with human perception DeepSeek-AI (2025), yet current RL-based QA methods employ scalar or rank-only rewards that fail to balance intra-sample calibration and inter-sample preference consistency. We argue that human perceptual evaluation inherently involves two complementary dimensions: (i) response consistency: coherence within the same perceptual context, and (ii) preference alignment: agreement across samples. Unifying them under a disentangled formulation can elicit multimodal reasoning and yield robust, interpretable quality assessment.

In this work, we propose **PreResQ-R1** (see Fig. 1), a **Preference-Response Disentangled Reinforcement Learning** framework for fine-grained visual quality assessment. PreResQ-R1 explicitly integrates long-chain reasoning CoT within a Group Relative Policy Optimization (GRPO) scheme to jointly optimize score accuracy and ranking consistency. The total reward consists of: (1) a Response-based Ranking Reward that enforces intra-sample coherence by aligning multiple generations of the same input, and (2) a Preference-based Ranking-Score Reward that captures inter-sample perceptual relations through magnitude-aware comparative consistency. This disentangled reward enables robust convergence without dataset-specific tuning. To extend beyond static imagery, we introduce a global-temporal and local-spatial data flow strategy for video quality assessment (VQA): all frames are compactly aggregated into a global multiframe representation to capture long-range temporal dynamics, while a few randomly sampled frames provide local spatial details. This hybrid design enables unified reasoning across spatial and temporal dimensions of perceptual quality. Finally, an Exploration-to-Stability Fine-tuning Strategy encourages diverse reasoning trajectories under multi-prompt perturbations and refines them via standard deviation regularization to suppress overconfident predictions. Extensive experiments demonstrate that PreResQ-R1 achieves state-of-the-art results across both IQA and VQA benchmarks under PLCC and SRCC metrics. Beyond quantitative gains, it generates human-aligned, fine-grained reasoning traces that reveal the perceptual cues underlying visual quality judgments.

## 2 RELATED WORK

### 2.1 REGRESSION-BASED MODELS

Classical IQA and VQA methods typically treat perceptual quality as an absolute regression problem. Early approaches such as PSNR Huynh-Thu & Ghanbari (2008), SSIM Wang et al. (2004), FSIM Zhang et al. (2011), and VIF Sheikh & Bovik (2006) relied on signal fidelity or handcrafted priors, while learning-based methods like BRISQUE Mittal et al. (2012) and NIQE Mittal et al. (2013) modeled natural scene statistics. With deep learning, CNN-based models (e.g., DBCNN Zhang et al. (2020), HyperIQA Su et al. (2020), MUSIQ Ke et al. (2021), and DOVER Wu

et al. (2023a)) and Transformer-based methods (Swin-IQA Wang et al. (2022), and FAST-VQA Wu et al. (2022)) achieved end-to-end quality prediction using regression losses. Recently, regression has been extended into vision-language models (VLMs). Works such as Q-Align Wu et al. (2023b), DeQA You et al. (2025), and Q-Insight Li et al. (2025) formulate IQA as a continuous regression task on top of multimodal representations, leveraging pretrained CLIP-like encoders for perceptual reasoning. These models demonstrate strong generalization but remain limited by the absolute nature of scalar regression, motivating a shift toward comparative and reasoning-based paradigms.

## 2.2 RANKING-BASED MODELS

Ranking-based IQA and VQA reframe quality assessment as a relative comparison problem more consistent with human perception. Early work such as RankIQA Liu et al. (2017), and PaQ-2-PiQ Ying et al. (2019) optimized pairwise or listwise order consistency (e.g., Spearman or Kendall correlation). In the multimodal era, ranking has become the preferred paradigm for quality evaluation within VLMs. Approaches such as Compare2Score Zhu et al. (2024), DeQA-Score You et al. (2025), Co-Instruct Wu et al. (2024), LMM-PVQA Cao et al. (2025b) and VisualQuality-R1 Wu et al. (2025) train MLLMs with comparative preference data, enabling fine-grained perceptual alignment and interpretable rationales. Unlike scalar regression, these models optimize differentiable ranking losses and learn to reason, effectively bridging subjective human judgments and visual-language embeddings.

## 2.3 REINFORCEMENT LEARNING-BASED MODELS

Reinforcement learning provides a mechanism to align MLLMs with human perceptual feedback. Inspired by RLHF Ouyang et al. (2022) and RLAIIF Yu et al. (2024a), recent works employ reward-based optimization to refine large models via GRPO Shao et al. (2024). This strategy underpins DeepSeek-R1-Zero DeepSeek-AI (2025), R1-VL Zhang et al. (2025a), and Visual-RFT Liu et al. (2025b), enabling self-improvement in multimodal reasoning without explicit human supervision. For quality assessment, RL-based alignment (Q-Insight Li et al. (2025), VQ-Insight Zhang et al. (2025b), and VQA-Thinker Cao et al. (2025a)) bridges reasoning and perceptual fidelity. Q-Insight Li et al. (2025) jointly optimizes score regression and degradation perception through GRPO, while VisualQuality-R1 Wu et al. (2025) reformulates IQA as a reasoning-guided ranking task with continuous reward modeling, achieving strong human-aligned performance. Related extensions such as VideoDPO Liu et al. (2024), VideoReward Liu et al. (2025a), and UnifiedReward Wang et al. (2025b) further demonstrate RL’s potential in visual preference alignment.

# 3 PROPOSED MODEL

## 3.1 OVERVIEW

This work aims to incorporate long CoT reasoning into the reward MLLM’s assessment process to enhance the robustness of reward signals. Empirical evidence shows that relying solely on score-based rewards often results in imbalanced score distributions, while rank-based rewards tend to be dataset-specific, leading to limitations in generalization across diverse tasks. The key challenge lies in devising an effective strategy to elicit and incentivize CoT capability. Therefore, we take the first step to proposed a preference-response disentangled multimodal CoT-based NR-QA model (see Fig. 2), PreResQ-R1, to activates and refines both score and rank convergence through fine-grained reasoning.

## 3.2 FINE-GRAINED REASONING CoT FOR IQA AND VQA

Given a text prompt  $\mathcal{P}$  and an image or video  $\mathcal{I}$  in an image/video quality dataset, our goal is to fine-tune a pretrained MLLM with parameters  $\theta$  and policy  $\pi_\theta(\cdot|\mathcal{P}, \mathcal{I})$  to generate quality reasoning trajectories  $\tau$  that provide a comprehensive CoT  $c$  along with an overall score  $s \in [1, 5]$ :

$$\tau = (c, s) \sim \pi_\theta(\cdot|\mathcal{P}, \mathcal{I}) \quad (1)$$

We present the complete structured text prompt in Appendix. For each image-score pair  $x_i = (\mathcal{P}_i, \mathcal{I}_i)$  in IQA, the MLLM generates detailed Chain-of-Thought (CoT) reasoning for five quality

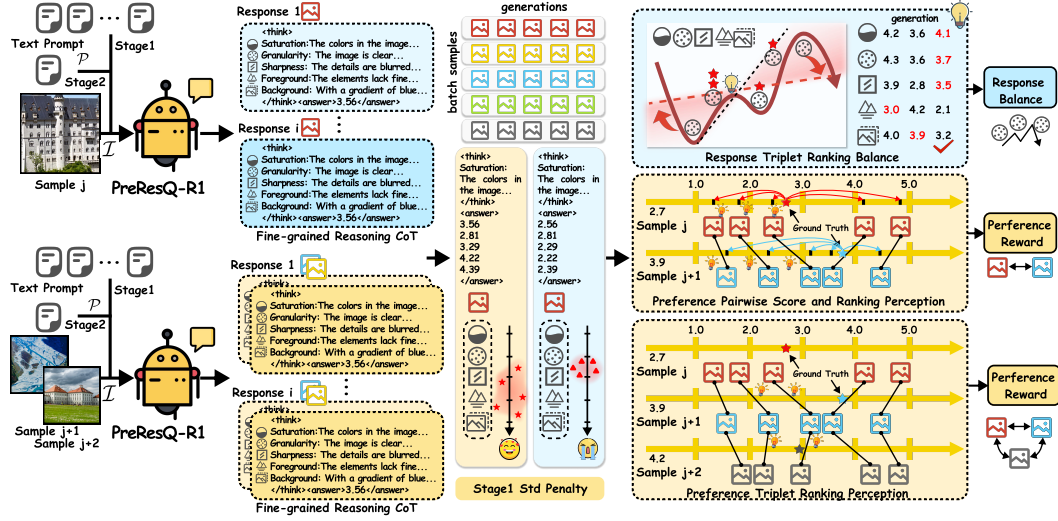


Figure 2: Overall training framework of PreResQ-R1 via RL2RS. Given an sample batch  $(\mathcal{I}_j, \mathcal{I}_{j+1}, \dots, \mathcal{I}_{j+B})$  with a shared text prompt  $\mathcal{P}$ , PreResQ-R1 generates  $K$  responses. To quickly activate CoT differences and then access generation stability, we introduce the response penalty and fine-grained triplet-response balance reward. To jointly enhance the robustness of ranking and score ability, we introduce the preference pairwise-and-triplet score-and-ranking reward for GRPO.

aspects: Saturation, Granularity, and Sharpness, which capture pixel-level properties, and Foreground and Background, which capture semantic-level information, followed by the corresponding numeric scores. For VQA, inspired by DeepSeek-OCR Wei et al. (2025), we represent the one temporal dimension image by shrinking all frames and stacking them into a single global multiframe image, while randomly selecting three frames as local single-frame spatial images. This design allows the model to jointly perceive both global temporal trends and local spatial details effectively. For every training batch of image/video-score pairs  $\{x_i, x_{i+1}, \dots, x_{i+B}\}$ , where  $B$  is the minibatch size, we apply GRPO to generate  $K$  quality predictions for  $x_i$ :

$$\tau(x_i) = [\tau_1(x_i), \tau_2(x_i), \dots, \tau_K(x_i)] \quad (2)$$

These multiple predictions naturally encode uncertainty, enabling reliable relative ranking and absolute score estimation across both IQA and VQA (see details in Appendix).

### 3.3 PREFERENCE-RESPONSE DISENTANGLED POLICY OPTIMIZATION (PRPO)

PRPO explicitly decomposes the reward into two complementary components that jointly capture the essence of perceptual reasoning. The **Response Dimension** focuses on intra-sample consistency, evaluating how coherently the model reasons across multiple generations of the same sample. Meanwhile, the **Preference Dimension** models inter-sample relations, encouraging the predicted quality ordering to align with human MOS. In addition, a format reward  $R_f$  is utilized to ensure specific reason and answer format. This disentangled formulation allows the reward to balance absolute judgment and relative preference, yielding a more stable and perceptually faithful optimization process.

#### 3.3.1 RESPONSE BASED RANKING REWARD (RR)

For an intra-generation triplet-wise group  $\mathcal{T}_{i,j,d} = \{\tau_{j,d}^l, \tau_{j,d}^m, \tau_{j,d}^n\}$ , with dimension index  $d \in [1, 5]$ , generation  $\{l, m, n\} \ni i$ , and sample index  $j$ , we denote the score prediction by  $s_{j,d}^l, s_{j,d}^m, s_{j,d}^n$ , we compute a geometric median-centered stabilizer:

$$\tilde{s}_d(\mathcal{T}_{i,j}) = \arg \min_{\xi} \sum_{t \in \{l, m, n\}} |s_{j,d}^t - \xi|, \quad (3)$$

which  $\xi$  softly represents the perceptual equilibrium within the triplet. The local alignment coefficient for sample  $j$  generation  $i$  on dimension  $d$  is then given by

$$\lambda_{i,j}^d = \frac{1}{|\mathcal{T}_i|} \sum_{|\mathcal{T}_i|} \exp[-\gamma |s_{j,d}^i - \tilde{s}_d(\mathcal{T}_{i,j})|], \quad (4)$$

where  $|\mathcal{T}_i|$  denotes the number of triplets involving  $j$ , and  $\gamma$  controls sensitivity to local deviations. Averaging across all  $D = 5$  perceptual dimensions yields

$$R_{\text{loc}}^{j,i} = \frac{1}{D} \sum_{d=1}^D \lambda_{i,j}^d, \quad (5)$$

which replaces the discrete median indicator with a continuous exponential affinity, providing differentiability.

### 3.3.2 PREFERENCE BASED RANKING-SCORE REWARD (PRS)

**Pairwise Comparative Reward:** In reinforcement fine-tuning, each sample yields multiple stochastic generations, introducing intra-sample variability that can obscure reward consistency. To mitigate this effect, we utilize an intra-sample sort like the response dimension, where the  $K$  average predicted scores  $\{s_j^1, \dots, s_j^K\}$  from 5 dimension index for each sample  $j$  are sorted in descending order, forming an ordered sequence  $\hat{s}_j^{(1)} \leq \hat{s}_j^{(2)} \leq \dots \leq \hat{s}_j^{(K)}$ . Subsequent cross-sample comparisons are then conducted on the  $i$ -th ranked generations  $\hat{s}_j^{(k)}$  and  $\hat{s}_{j+1}^{(i)}$ , ensuring that preference evaluation operates over a consistent ordinal basis. This ranking-based formulation effectively disentangles generation noise from inter-sample preference learning, providing a stable foundation for the PRS. Formally, let  $\hat{s}_j^{(i)}$  denote the  $i$ -th order statistic of sample  $j$ 's predictions after intra-sample sorting, and let  $\mathbf{G}_j$  denote the ground-truth MOS. For any pair  $(l, m)$ , we measure pairwise ranking agreement between  $\hat{s}_l^{(i)}$  and  $\hat{s}_m^{(i)}$  with respect to  $(\mathbf{G}_l, \mathbf{G}_m)$ :

$$C_{l,m}^{(i)} = \begin{cases} 1, & \text{sign}(\hat{s}_l^{(i)} - \hat{s}_m^{(i)}) = \text{sign}(\mathbf{G}_l - \mathbf{G}_m), \\ 0, & \text{otherwise,} \end{cases} \quad (6)$$

which flags whether the  $i$ -th ranked generation preserves the ground-truth ordering. While intra-sample ranking mitigates permutation variance, ordinal consistency alone fails to reflect absolute quality differences. To enhance score sensitivity, we introduce a magnitude-aware alignment that softly measures the prediction-ground-truth consistency:

$$M_{l,m}^i = \frac{|\mathbf{G}_l - \mathbf{G}_m|}{|g_l - g_m| + |s_l^i - \mathbf{G}_l| + |s_m^i - \mathbf{G}_m|}, \quad (7)$$

where the numerator encodes the perceptual contrast between two samples, while the denominator balances deviations of predicted scores from their human-grounded references. Integrating ranking correctness and confidence, the smooth pairwise comparative reward is expressed as:

$$R_{\text{pair}}^{l,i} = \frac{1}{B-1} \sum_{l \neq m} \left[ \sqrt{C_{l,m}^i e^{M_{l,m}^i}} + \sqrt{(1 - C_{l,m}^i) e^{-(1+M_{l,m}^i)}} \right], \quad (8)$$

**Triplet Comparative Reward:** To capture higher-order consistency beyond pairwise comparisons, we introduce a triplet-based reward that enforces transitive ranking among three samples. For each anchor sample  $a$ , we construct the set of all triplets  $\mathcal{T}_i = \{(l, m, n) \mid m, n \neq l\}$ . For a single triplet  $(l, m, n) \in \mathcal{T}_i$ , the triplet reward is defined as:

$$r_{\text{tri}}^{(l,m,n),i} = \begin{cases} 1.0, & \text{if } C_{l,m}^{(i)} + C_{l,n}^{(i)} + C_{m,n}^{(i)} = 3, \\ 0.3, & \text{otherwise,} \end{cases} \quad (9)$$

where  $C_{l,m}^i \in \{0, 1\}$  denotes the pairwise consistency between predictions  $s_l^k, s_m^k$  and ground-truth scores  $\mathbf{G}_l, \mathbf{G}_m$ . The overall triplet reward for generation  $i$  and sample  $j$  is then computed as the mean over all triplets:

$$R_{\text{tri}}^{j,i} = \frac{1}{|\mathcal{T}_j|} \sum_{(l,m,n) \in \mathcal{T}_j} r_{\text{tri}}^{(l,m,n),i}. \quad (10)$$

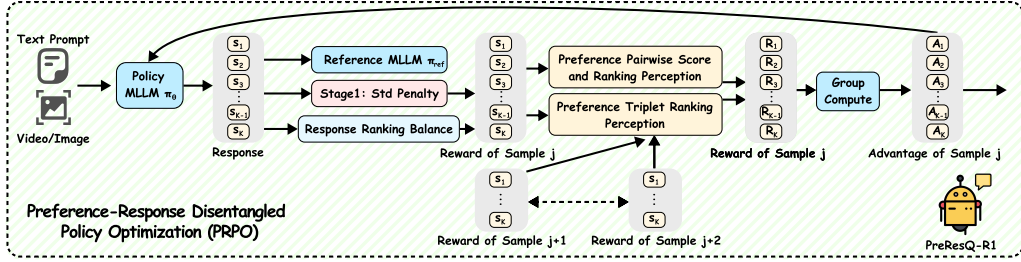


Figure 3: Pipeline of the Preference-Response Disentangled Policy Optimization (PRPO), which applies response ranking response balance reward, and preference pairwise score and ranking reward, and preference triplet ranking reward to optimize group policy learning.

**Unified Objective:** The total reward unifies the intra-response fidelity and cross-preference:

$$R_{\text{total}}^{j,i} = R_{\text{for}}^{j,i} + \alpha R_{\text{loc}}^{j,i} + (1 - \alpha) (\beta_1 R_{\text{pair}}^{j,i} + \beta_2 R_{\text{tri}}^{j,i}), \quad (11)$$

where  $\alpha \in [0, 1]$  balances local response and preference rewards, and  $\beta_1, \beta_2$  control the relative contributions of pairwise and triplet components. For reinforcement fine-tuning, we collect the  $K$  generated trajectories for each sample  $i$  into a reward vector:

$$r(s_j) = [R_{\text{total}}^{j,1}, R_{\text{total}}^{j,2}, \dots, R_{\text{total}}^{j,K}]^\top, \quad (12)$$

and define the relative advantage of the  $k$ -th trajectory as:

$$a(s_j^{(i)}) = r(s_j) - \mu(r(s_j)) / \sigma(r(s_j)), \quad (13)$$

where  $\mu(\cdot)$  and  $\sigma(\cdot)$  denote the mean and standard deviation over the  $K$  trajectories of sample  $j$ . The policy  $\pi_\theta(\cdot|c, s_j)$  is updated via a regularized GRPO objective that combines reward-weighted likelihood with KL divergence to a reference policy  $\pi_{\text{ref}}$  obtained from pretrained MLLM (see Fig. 3):

$$\begin{aligned} \mathcal{L}(\theta) = & \frac{1}{BK} \sum_{j=1}^B \sum_{i=1}^K \min \left[ \frac{\pi_\theta(o_i|c, s_j)}{\pi_\theta^{\text{old}}(o_i|c, s_j)} a(s_j^{(i)}), \right. \\ & \left. \text{clip} \left( \frac{\pi_\theta(o_i|c, s_j)}{\pi_\theta^{\text{old}}(o_i|c, s_j)}, 1 - \epsilon, 1 + \epsilon \right) a(s_j^{(i)}) \right] \\ & - \beta D_{\text{KL}}(\pi_\theta(o_i|c, s_j) \| \pi_{\text{ref}}(o_i|c, s_j)), \end{aligned} \quad (14)$$

where  $\epsilon$  is the clipping threshold, and  $\beta$  balances the regularization strength. The KL term is approximated as:

$$D_{\text{KL}}(\pi_\theta \| \pi_{\text{ref}}) \approx \pi_{\text{ref}} \frac{\pi_\theta}{\pi_{\text{ref}}} - \log \frac{\pi_\theta}{\pi_{\text{ref}}} - 1, \quad (15)$$

ensuring that the updated policy does not deviate excessively from the stable pretrained reference. We utilize policy gradient methods to optimize the MLLM by maximizing the expected cumulative reward  $R_{\text{total}}$  on sampled aesthetic reasoning trajectories  $J(\theta) = \mathbb{E}_{\tau \sim \pi_\theta(\cdot|\mathcal{P}, \mathcal{I})} [R_{\text{total}}]$ :

$$\nabla_\theta J(\theta) = \mathbb{E}_{\tau \sim \pi_\theta(\cdot|\mathcal{P}, \mathcal{I})} [R_{\text{total}} \sum_{t=1}^T \nabla_\theta \log \pi_\theta(a_t | s_t)] \quad (16)$$

where  $a_t$  is selected from the vocabulary space, and  $s_t = (\mathcal{P}, \mathcal{I}, a_{<t})$  represents the state at step  $t$ .

### 3.4 EXPLORATION-TO-STABILITY FINE-TUNING STRATEGY

To balance exploration and stable fine-tuning, we adopt a two-stage fine-tuning strategy. In the exploration stage ( $\tau$ ), each sample is paired with  $X$  randomly sampled prompts, encouraging the model to generate diverse trajectories. For each generation, we extract the five-dimensional scores  $\mathbf{s}_j^{(i)}$  and compute a dimension-wise standard deviation penalty:

$$R_{\text{std}}(\mathbf{s}_j^{(i)}) = \begin{cases} \lambda_{\text{std}}(\delta_{\text{min}} - \sigma(\mathbf{s}_j^{(i)})), & \sigma(\mathbf{s}_j^{(i)}) < \delta_{\text{min}}, \\ 0, & \text{otherwise,} \end{cases} \quad (17)$$

Table 1: Performance comparison of PreResQ-R1 across IQA datasets under SRCC and PLCC metrics. Red, green, and blue represent the Handcrafted, Discriminative deep-learning-based, and MLLM-based methods. **Bold** and underlined denote the best and second best.

Method	BID	CLIVE	KonIQ	SPAQ	KADID	Liu13	SRIQA	TID13	PIPAL	AGIQA	Avg
<b>Spearman's Rank Correlation Coefficient (SRCC)</b>											
BRISQUE Mittal et al. (2012)	0.522	0.314	0.385	0.614	0.429	0.389	0.210	0.548	0.242	0.497	0.415
NIQE Mittal et al. (2013)	0.515	0.450	0.421	0.676	0.487	0.360	0.194	0.532	0.357	0.533	0.453
MUSIQ Ke et al. (2021)	0.327	0.284	0.473	0.720	0.647	0.656	0.309	0.670	0.317	0.494	0.490
UNIQUE Zhang et al. (2021)	0.412	0.470	0.649	0.751	0.513	0.669	0.244	0.703	0.393	0.608	0.541
MANIQA Yang et al. (2022)	0.420	0.487	0.213	0.745	0.760	0.726	0.297	0.589	0.338	0.422	0.500
Qwen2.5-VL-7B Bai et al. (2025)	0.711	0.733	0.754	0.848	0.787	<u>0.840</u>	0.495	0.787	0.390	0.735	0.708
LIQE Zhang et al. (2023)	0.677	0.719	0.684	0.815	0.809	0.797	0.447	0.718	0.371	0.653	0.669
DeQA-Score You et al. (2025)	0.702	0.743	0.677	0.852	0.831	0.785	<u>0.579</u>	0.756	0.383	0.738	0.705
Q-Align Wu et al. (2023c)	0.576	0.554	0.573	0.767	0.832	0.761	0.421	0.769	0.406	0.682	0.634
UnifiedReward-T Wang et al. (2025a)	0.745	0.738	0.820	0.871	0.841	0.809	0.462	0.788	0.399	0.722	0.720
Q-Insight Li et al. (2025)	0.784	<u>0.761</u>	0.806	<u>0.892</u>	0.856	0.831	0.525	0.816	0.429	0.749	0.745
VisualQuality-R1 Wu et al. (2025)	<u>0.790</u>	0.750	<u>0.855</u>	0.875	<u>0.871</u>	<u>0.838</u>	0.561	<u>0.848</u>	<u>0.469</u>	<u>0.805</u>	0.768
PreResQ-R1 (Ours)	<b>0.849</b>	<b>0.825</b>	<b>0.884</b>	<b>0.919</b>	<b>0.894</b>	<b>0.873</b>	<b>0.601</b>	<b>0.858</b>	<b>0.588</b>	<b>0.823</b>	<b>0.811</b>
<b>Pearson Linear Correlation Coefficient (PLCC)</b>											
BRISQUE Mittal et al. (2012)	0.528	0.362	0.400	0.624	0.451	0.380	0.163	0.546	0.259	0.541	0.425
NIQE Mittal et al. (2013)	0.527	0.494	0.439	0.683	0.415	0.376	0.135	0.516	0.314	0.560	0.446
MUSIQ Ke et al. (2021)	0.280	0.325	0.435	0.666	0.622	0.563	0.283	0.695	0.347	0.434	0.456
UNIQUE Zhang et al. (2021)	0.385	0.472	0.590	0.708	0.548	0.654	0.207	0.729	0.361	0.581	0.524
MANIQA Yang et al. (2022)	0.512	0.571	0.257	0.753	0.780	0.728	0.289	0.617	0.364	0.448	0.532
Qwen2.5-VL-7B Bai et al. (2025)	0.725	0.760	0.810	0.854	0.806	0.852	0.504	0.837	0.420	0.772	0.734
LIQE Zhang et al. (2023)	0.680	0.726	0.652	0.814	0.817	0.712	0.430	0.748	0.347	0.653	0.658
DeQA-Score You et al. (2025)	0.743	<u>0.795</u>	0.703	0.858	0.873	0.838	<u>0.589</u>	0.793	0.381	0.743	0.732
Q-Align Wu et al. (2023c)	0.651	0.643	0.612	0.779	0.862	0.802	0.459	0.794	0.381	0.694	0.668
UnifiedReward-T Wang et al. (2025a)	0.767	0.795	0.804	0.846	0.877	0.835	0.518	<u>0.873</u>	0.421	0.745	0.748
Q-Insight Li et al. (2025)	0.796	<u>0.795</u>	0.829	0.872	<u>0.881</u>	0.857	0.542	0.851	<b>0.485</b>	0.794	0.770
VisualQuality-R1 Wu et al. (2025)	<u>0.806</u>	0.794	<u>0.840</u>	<u>0.878</u>	0.821	<b>0.872</b>	0.543	0.871	0.458	<b>0.843</b>	0.773
PreResQ-R1 (Ours)	<b>0.839</b>	<b>0.825</b>	<b>0.887</b>	<b>0.900</b>	<b>0.892</b>	<u>0.864</u>	<b>0.596</b>	<b>0.877</b>	<u>0.431</u>	<u>0.809</u>	<b>0.790</b>

Table 2: Performance comparison of PreResQ-R1 across different VQA datasets under SRCC and PLCC metrics. Red, green, and blue represent the Handcrafted, Discriminative Deep-learning, and MLLM-based methods, respectively. **Bold** and underlined denote the best and second best.  $\circ$ ,  $\diamond$ ,  $\star$  represent the fused-287K, VQA<sup>2</sup>-157K, LSVQ-KonIQ-38K, LSVQ-28K training data, respectively.

Method	LSVQ <sub>test</sub>		LSVQ <sub>1080p</sub>		KoNVid-1k		LIVE-VQC		YouTube-UGC		Avg	
	SRCC	PLCC	SRCC	PLCC	SRCC	PLCC	SRCC	PLCC	SRCC	PLCC	SRCC	PLCC
STEM Kancharla & Channappayya (2022) $\star$	0.206	0.243	0.434	0.381	0.619	0.627	0.594	0.629	0.284	0.318	0.427	0.440
NIQE Mittal et al. (2013) $\star$	0.442	0.332	0.489	0.459	0.541	0.553	0.596	0.628	0.278	0.290	0.469	0.452
FAST-VQA Wu et al. (2022) $\star$	0.880	0.880	0.781	0.813	0.859	0.854	<b>0.826</b>	0.845	0.730	0.747	0.833	0.828
MinimalisticVQA Sun et al. (2024) $\star$	0.885	0.882	0.792	0.828	0.862	0.859	0.775	0.821	0.826	0.821	0.828	0.842
Q-Align Wu et al. (2023c) $\circ$	<u>0.886</u>	<u>0.884</u>	0.761	0.822	0.876	0.878	0.783	0.819	0.834	0.846	0.828	0.850
VQA <sup>2</sup> -Scorer Jia et al. (2024) $\diamond$	0.878	0.872	<u>0.794</u>	0.821	0.881	0.880	0.785	0.830	<b>0.811</b>	0.823	0.830	0.845
Q-Insight Li et al. (2025) $\star$	0.644	0.639	0.601	0.648	0.751	0.753	0.624	0.708	0.560	0.591	0.636	0.668
VisualQuality-R1 Wu et al. (2025)	0.795	0.796	0.716	0.744	0.784	0.792	0.732	0.781	0.717	0.730	0.749	0.769
VQ-Insight Zhang et al. (2025b) $\triangleleft$	0.875	0.876	0.786	0.823	0.875	0.884	0.790	0.835	-	-	-	-
VQAThinker Cao et al. (2025a) $\star$	0.883	0.880	<b>0.798</b>	<b>0.834</b>	<b>0.881</b>	<u>0.884</u>	0.808	<u>0.847</u>	<u>0.860</u>	<b>0.863</b>	0.846	0.862
PreResQ-R1 (Ours) $\star$	<b>0.901</b>	<b>0.893</b>	0.794	0.825	<u>0.879</u>	<b>0.889</b>	<u>0.812</u>	<b>0.849</b>	<b>0.866</b>	<u>0.857</u>	<b>0.850</b>	<b>0.863</b>

where  $\mathbf{s}_j^{(i)} = [s_j^1, \dots, s_j^5]$  denotes the five-dimensional quality scores for the  $i$ -th generation of sample  $j$ , and  $\sigma(\mathbf{s}_j^{(i)})$  is the standard deviation across these five scores.

## 4 EXPERIMENT

### 4.1 EXPERIMENTAL SETUPS

For IQA task, PreResQ-R1 is trained exclusively on the synthetic KADID-10K dataset (6:2:2 split in content independence) and tested in a zero-shot setting across ten open-source general (real-world and AI-generated) image aesthetic assessment datasets: BID Ciancio et al. (2011), CLIVE Ghadiyaram & Bovik (2016), KonIQ-10k Hosu et al. (2020b), SPAQ Fang et al. (2020), KADID Lin et al. (2019), Liu 13 Liu et al. (2013), SRIQA-Bench Chen et al. (2025a), AGIQA-3K Li et al. (2023), TID 2013 PON (2015), and PIPAL Gu et al. (2020). For VQA task, PreResQ-R1 is trained exclusively on the LSVQ-28K Ying et al. (2021) dataset and test in a zero-shot setting across five open-source in-domain UGC videos with in-the-wild distortions: LSVQ<sub>test</sub> Ying et al. (2021), LSVQ<sub>1080p</sub> Ying et al. (2021), KoNVid-1k Hosu et al. (2020a), LIVE-VQC Sinno & Bovik (2019), YouTube-UGC Wang et al. (2019).

Table 3: Performance ablation of PreResQ-R1 across different reward functions. RTR, PSR, and PTR represent the Response Triplet Ranking reward, Preference Pairwise Score and Ranking reward, and Preference Triplet Ranking reward, respectively.

RTR	PSR	PTR	BID		KonIQ		SPAQ		Liu13		TID2013		AGIQA	
			PLCC	SRCC										
✗	✓	✗	0.782	0.767	0.839	0.859	0.844	0.834	0.857	0.816	0.775	0.796	0.762	0.759
✗	✗	✓	0.765	0.790	0.868	0.875	0.858	0.829	0.847	0.856	0.794	0.781	0.770	0.764
✓	✓	✗	0.795	0.813	0.872	0.867	0.882	0.890	<b>0.877</b>	0.864	0.823	0.847	0.791	0.808
✓	✗	✓	0.816	0.809	<b>0.895</b>	<b>0.904</b>	0.896	0.889	0.868	<b>0.875</b>	0.842	0.858	0.785	0.779
✓	✓	✓	<b>0.849</b>	<b>0.839</b>	0.884	0.887	<b>0.919</b>	<b>0.900</b>	0.873	0.864	<b>0.858</b>	<b>0.877</b>	<b>0.823</b>	<b>0.809</b>

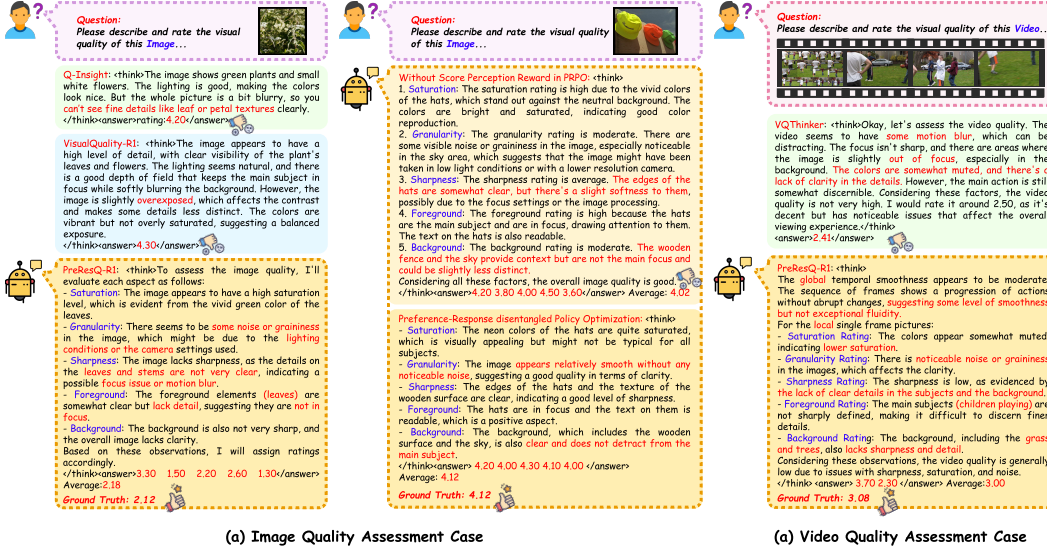


Figure 4: (a) Qualitative cases of IQA in comparison and ablation studies. (b) Qualitative cases of VQA in comparison studies.

## 4.2 IMPLEMENTATION DETAILS

We compare our method with HandCrafted methods (BRISQUE Mittal et al. (2012), NIQE Mittal et al. (2013), STEM Kancharla & Channappayya (2022)), discriminative deep-learning methods (MUSIQ Ke et al. (2021), UNIQUE Zhang et al. (2021), MANIQA Yang et al. (2022), FAST-VQA Wu et al. (2022), MinimalisticVQA Sun et al. (2024)), and MLLM based methods (Qwen2.5-VL-7B Bai et al. (2025), LIQE, DeQA-Score You et al. (2025), Q-Align Wu et al. (2023c), UnifiedReward-T Wang et al. (2025a), Q-Insight Li et al. (2025), VisualQuality-R1 Wu et al. (2025), VQA<sup>2</sup>-Scorer Jia et al. (2024), VQ-Insight Zhang et al. (2025b), VQAThinker Cao et al. (2025a)). We conduct IQA PreResQ-R1 in two stages. In the first stage, prompts are randomly selected from a predefined set of  $\mathbf{X} = 5$ , with standard deviation (std) penalties set as  $\delta_{\min} = 0.5$  and  $\lambda_{\text{std}} = 0.5$ , and generate  $K = 12$  responses each sample. In the second stage, we generate  $K = 6$  responses each sample. We set  $\beta_1=0.375$ ,  $\beta_2=0.125$ ,  $\alpha=0.5$ . We fine-tune Qwen2.5-VL-7B Bai et al. (2025) with GRPO Shao et al. (2024) without freezing any layers. For VQA task, we set  $K = 5$  and PreResVQA-R1 fine-tuned based on the PreResQA-R1 only in single-prompt stage. Training is performed using AdamW Loshchilov & Hutter (2019) with an initial learning rate of  $3 \times 10^{-7}$ , a linear decay schedule. Experiments are conducted on 8 NVIDIA A800 GPUs with a per-GPU batch size of 48 for the IQA task and 25 for the VQA task. Training takes 8 epochs for IQA and 1 epoch for VQA, requiring about 20 hours and 35 hours.

## 4.3 COMPARISON STUDIES

For IQA task, we conduct both qualitative and quantitative comparisons with handcrafted, discriminative deep-learning, and MLLM-based IQA methods, as summarized in Table 1. PreResQ-R1 achieves an average SRCC of **0.811** and PLCC of **0.795** across ten benchmark datasets, surpassing

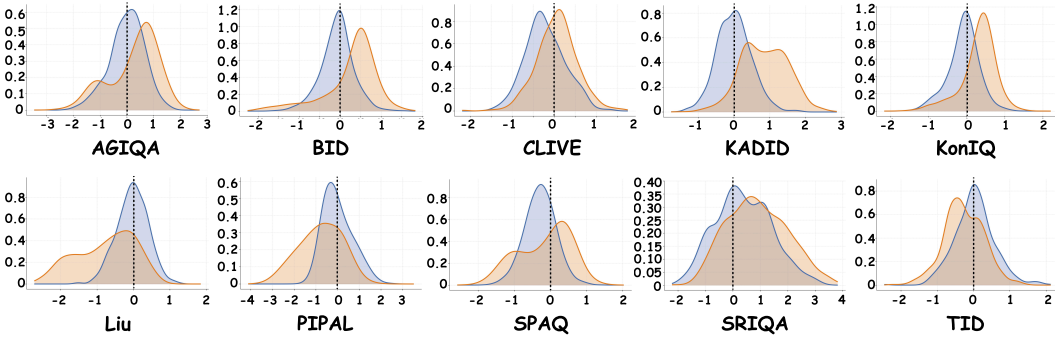


Figure 5: Comparison between PreResQ-R1 and VisualQuality-R1 on distribution of difference between answer and ground truth. The horizontal axis represents the error, and the vertical axis represents the relative proportion. The closer the distribution is to 0, the better the model performance is. Blue and Orange represents PreResQ-R1 and VisualQuality-R1.

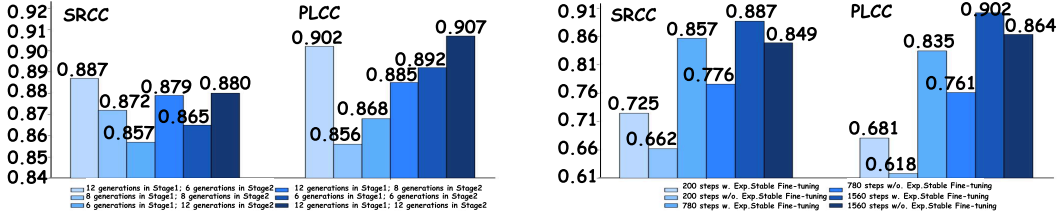


Figure 6: Left: Performance on synthetic ten evaluation datasets (each dataset 100 images) with different generation number across two stages on SRCC and PLCC metrics; Right: Performance on evaluation datasets with/without Exploration-to-Stability Fine-tuning Strategy.

previous approaches by **5.6%** and **2.2%**, respectively. Notably, PreResQ-R1 attains the best SRCC performance across all datasets, benefiting from the proposed pairwise-triplet score-ranking reward in PRPO. Furthermore, quantitative analyses of the prediction-ground-truth error distributions indicate that PreResQ-R1 produces consistently smaller deviations than VisualQuality-R1 across all test sets. As shown in Fig. 4(a), qualitative case comparisons further demonstrate that PreResQ-R1 provides more accurately aligned quality descriptions and finer-grained reasoning processes compared to Q-Insight and VisualQuality-R1, which occasionally hallucinate by misjudging deceptively low-quality images as high-quality ones (see Appendix for more details). To extend beyond imagery, we conduct both qualitative and quantitative comparisons with comparable methods in VQA task, as summarized in Table 2. PreResQ-R1 achieves an average SRCC of **0.850** and PLCC of **0.863** across five benchmark datasets, surpassing previous state-of-the-art methods. Furthermore, the quantitative case shown in Fig. 4(b) demonstrates that, compared with VQ-Thinker, PreResQ-R1 produces more accurate scores while providing more comprehensive reasoning that covers both global-temporal and local-spatial aspects, as well as fine-grained attributes including saturation, granularity, sharpness, foreground, and background. Such fine-grained CoT is particularly crucial for human perceptual tasks, providing deeper insights into how MLLM aligns with human judgment (see Appendix for details).

#### 4.4 ABLATION STUDIES

We further conduct qualitative and quantitative ablation studies on the IQA task to examine the effects of different preference-response disentangled policy optimization rewards, as summarized in Table 3. Using only the Preference Pairwise Score and Ranking (PSR) or Preference Triplet Ranking (PTR) rewards leads to suboptimal performance, as shown in the first two rows. When the Response Triplet Ranking (RTR) reward is incorporated, the model exhibits a clear improvement, as presented in the third and fourth rows. Finally, combining all three reward functions within the proposed PRPO framework yields the best overall performance across most datasets, indicating that these objectives are complementary and mutually reinforcing. Moreover, we provide ad-

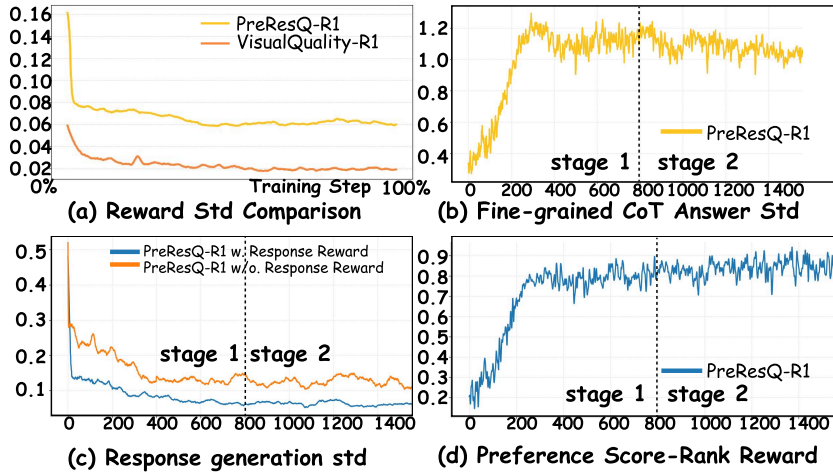


Figure 7: (a). Reward standard deviation comparison between VisualQuality-R1 and PreResQ-R1. (b). Fine-grained CoT answer intra standard deviation. (c). generation standard deviation comparison. (d). Preference Score-Rank Reward visualization.

ditional absolute-score-relative-rank ablation qualitative studies on the IQA task in Fig.4 (a) and global-temporal-local-spatial analyses on the VQA task in the Appendix. Without the score perception reward, the reasoning chain-of-thought becomes less coherent and the score of IQA degrades significantly, demonstrating the rationality and necessity of the PreResQ-R1 model design.

#### 4.5 COMPREHENSIVE STUDIES

We conduct comprehensive analyses on generation number, the Exploration-to-Stability Fine-tuning Strategy (ESS), and training dynamics, using 100 randomly sampled images per IQA dataset. Fig. 6(a) shows that response generation numbers in both stages significantly affect performance: generating more responses in Stage 1 while balancing generation and comparison samples in Stage 2 yields optimal results. Fig. 6(b) demonstrates that ESS accelerates convergence and improves multi-granularity prediction accuracy, achieving final scores of 88.7% and 90.2%, compared with 84.9% and 86.4% without ESS after 1560 steps. Fig. 7 visualizes training dynamics, including reward std compared with VisualQuality-R1, fine-grained CoT answer std under std penalty, response generation std with RTR ablation, and preference score-rank reward across steps. Reward std analysis in Fig. 7(a) indicates that PreResQ-R1 moves beyond a single stable target toward discriminative pairwise and triplet preference fitting. The CoT answer std curve in Fig. 7(b) demonstrates rapid differentiation across granularity levels enabled by std penalty. Introducing RTR further stabilizes response generation std for consistent optimization in Fig. 7(c). Finally, Fig. 7(d) shows progressive stabilization and improvement of the preference score-rank reward throughout training.

## 5 CONCLUSION AND FUTURE WORK

We introduced PreResQ-R1, a preference-response disentangled reinforcement learning framework that unifies score regression and ranking consistency via reasoning-driven optimization. With only 6K samples and 28K samples, it achieves state-of-the-art performance across 10 IQA datasets and 5 VQA datasets while providing interpretable CoT process. Future work will aim to integrate image quality assessment with text-to-image generation within a unified framework, enabling complementary optimization between visual generation and perceptual evaluation toward more consistent and human-aligned visual understanding.

## REFERENCES

- Image database tid2013: Peculiarities, results and perspectives. *Signal Processing: Image Communication*, 30:57–77, 2015. ISSN 0923-5965. doi: <https://doi.org/10.1016/j.image.2014.10.009>. URL <https://www.sciencedirect.com/science/article/pii/S0923596514001490>.
- Shuai Bai, Keqin Chen, Xuejing Liu, Jialin Wang, Wenbin Ge, Sibao Song, Kai Dang, Peng Wang, Shijie Wang, Jun Tang, Humen Zhong, Yuanzhi Zhu, Mingkun Yang, Zhaohai Li, Jianqiang Wan, Pengfei Wang, Wei Ding, Zheren Fu, Yiheng Xu, Jiabo Ye, Xi Zhang, Tianbao Xie, Zesen Cheng, Hang Zhang, Zhibo Yang, Haiyang Xu, and Junyang Lin. Qwen2.5-vl technical report, 2025. URL <https://arxiv.org/abs/2502.13923>.
- Xin Cai, Zhiyuan You, Hailong Zhang, Wentao Liu, Jinwei Gu, and Tianfan Xue. Phocolens: Photorealistic and consistent reconstruction in lensless imaging, 2024. URL <https://arxiv.org/abs/2409.17996>.
- Linhan Cao, Wei Sun, Weixia Zhang, Xiangyang Zhu, Jun Jia, Kaiwei Zhang, Dandan Zhu, Guangtao Zhai, and Xiongkuo Min. Vqathinker: Exploring generalizable and explainable video quality assessment via reinforcement learning, 2025a. URL <https://arxiv.org/abs/2508.06051>.
- Linhan Cao, Wei Sun, Xiangyang Zhu, Kaiwei Zhang, Jun Jia, Yicong Peng, Dandan Zhu, Guangtao Zhai, and Xiongkuo Min. Towards generalized video quality assessment: A weak-to-strong learning paradigm, 2025b. URL <https://arxiv.org/abs/2505.03631>.
- Du Chen, Tianhe Wu, Kede Ma, and Lei Zhang. Toward generalized image quality assessment: Relaxing the perfect reference quality assumption, 2025a. URL <https://arxiv.org/abs/2503.11221>.
- Zijian Chen, Wei Sun, Haoning Wu, Zicheng Zhang, Jun Jia, Ru Huang, Xiongkuo Min, Guangtao Zhai, and Wenjun Zhang. Study of subjective and objective naturalness assessment of ai-generated images. *IEEE Transactions on Circuits and Systems for Video Technology*, 35(4):3573–3588, 2025b. doi: 10.1109/TCSVT.2024.3509032.
- Zixuan Chen, Zewei He, Ziqian Lu, Xuecheng Sun, and Zhe-Ming Lu. Prompt-based test-time real image dehazing: a novel pipeline, 2024. URL <https://arxiv.org/abs/2309.17389>.
- Alexandre Ciancio, André Luiz N Targino Targino da Costa, Eduardo A. B. da Silva, Amir Said, Ramin Samadani, and Pere Obrador. No-reference blur assessment of digital pictures based on multifeature classifiers. *IEEE Transactions on Image Processing*, 20(1):64–75, 2011. doi: 10.1109/TIP.2010.2053549.
- DeepSeek-AI. Deepseek-r1: Incentivizing reasoning capability in llms via reinforcement learning, 2025. URL <https://arxiv.org/abs/2501.12948>.
- Yuming Fang, Hanwei Zhu, Yan Zeng, Kede Ma, and Zhou Wang. Perceptual quality assessment of smartphone photography. In *2020 IEEE/CVF Conference on Computer Vision and Pattern Recognition (CVPR)*, pp. 3674–3683, 2020. doi: 10.1109/CVPR42600.2020.00373.
- Deepti Ghadiyaram and Alan C. Bovik. Massive online crowdsourced study of subjective and objective picture quality. *IEEE Transactions on Image Processing*, 25(1):372–387, 2016. doi: 10.1109/TIP.2015.2500021.
- Jinjin Gu, Haoming Cai, Haoyu Chen, Xiaoxing Ye, Jimmy Ren, and Chao Dong. Pipal: a large-scale image quality assessment dataset for perceptual image restoration, 2020. URL <https://arxiv.org/abs/2007.12142>.
- Vlad Hosu, Hanhe Lin, Tamas Sziranyi, and Dietmar Saupe. Koniq-10k: An ecologically valid database for deep learning of blind image quality assessment. *Trans. Img. Proc.*, 29: 4041–4056, January 2020a. ISSN 1057-7149. URL <https://doi.org/10.1109/TIP.2020.2967829>.

- Vlad Hosu, Hanhe Lin, Tamas Sziranyi, and Dietmar Saupe. Koniq-10k: An ecologically valid database for deep learning of blind image quality assessment. *IEEE Transactions on Image Processing*, 29:4041–4056, 2020b. ISSN 1941-0042. doi: 10.1109/tip.2020.2967829. URL <http://dx.doi.org/10.1109/TIP.2020.2967829>.
- Q. Huynh-Thu and M. Ghanbari. Scope of validity of psnr in image/video quality assessment. *Electronics Letters*, 44:800–801, 2008. doi: 10.1049/el:20080522.
- Ziheng Jia, Zicheng Zhang, Jiaying Qian, Haoning Wu, Wei Sun, Chunyi Li, Xiaohong Liu, Weisi Lin, Guangtao Zhai, and Xiongkuo Min. Vqa<sup>2</sup>: Visual question answering for video quality assessment, 2024. URL <https://arxiv.org/abs/2411.03795>.
- Parimala Kancharla and Sumohana S. Channappayya. Completely blind quality assessment of user generated video content. *IEEE Transactions on Image Processing*, 31:263–274, 2022. doi: 10.1109/TIP.2021.3130541.
- Junjie Ke, Qifei Wang, Yilin Wang, Peyman Milanfar, and Feng Yang. Musiq: Multi-scale image quality transformer. In *2021 IEEE/CVF International Conference on Computer Vision (ICCV)*, pp. 5128–5137, 2021. doi: 10.1109/ICCV48922.2021.00510.
- Chunyi Li, Zicheng Zhang, Haoning Wu, Wei Sun, Xiongkuo Min, Xiaohong Liu, Guangtao Zhai, and Weisi Lin. Agiqa-3k: An open database for ai-generated image quality assessment, 2023. URL <https://arxiv.org/abs/2306.04717>.
- Weiqi Li, Xuanyu Zhang, Shijie Zhao, Yabin Zhang, Junlin Li, Li Zhang, and Jian Zhang. Q-insight: Understanding image quality via visual reinforcement learning, 2025. URL <https://arxiv.org/abs/2503.22679>.
- Hanhe Lin, Vlad Hosu, and Dietmar Saupe. Kadid-10k: A large-scale artificially distorted iqa database. In *2019 Eleventh International Conference on Quality of Multimedia Experience (QoMEX)*, pp. 1–3, 2019. doi: 10.1109/QoMEX.2019.8743252.
- Jie Liu, Gongye Liu, Jiajun Liang, Ziyang Yuan, Xiaokun Liu, Mingwu Zheng, Xiele Wu, Qiulin Wang, Wenyu Qin, Menghan Xia, Xintao Wang, Xiaohong Liu, Fei Yang, Pengfei Wan, Di Zhang, Kun Gai, Yujiu Yang, and Wanli Ouyang. Improving video generation with human feedback, 2025a. URL <https://arxiv.org/abs/2501.13918>.
- Runtao Liu, Haoyu Wu, Zheng Ziqiang, Chen Wei, Yingqing He, Renjie Pi, and Qifeng Chen. Videodpo: Omni-preference alignment for video diffusion generation, 2024. URL <https://arxiv.org/abs/2412.14167>.
- Xialei Liu, Joost van de Weijer, and Andrew D. Bagdanov. Rankiqa: Learning from rankings for no-reference image quality assessment, 2017. URL <https://arxiv.org/abs/1707.08347>.
- Yiming Liu, Jue Wang, Sunghyun Cho, Adam Finkelstein, and Szymon Rusinkiewicz. A no-reference metric for evaluating the quality of motion deblurring. *ACM Trans. Graph.*, 32(6), November 2013. ISSN 0730-0301. doi: 10.1145/2508363.2508391. URL <https://doi.org/10.1145/2508363.2508391>.
- Ziyu Liu, Zeyi Sun, Yuhang Zang, Xiaoyi Dong, Yuhang Cao, Haodong Duan, Dahua Lin, and Jiaqi Wang. Visual-rft: Visual reinforcement fine-tuning, 2025b. URL <https://arxiv.org/abs/2503.01785>.
- Ilya Loshchilov and Frank Hutter. Decoupled weight decay regularization, 2019. URL <https://arxiv.org/abs/1711.05101>.
- Anish Mittal, Anush Krishna Moorthy, and Alan Conrad Bovik. No-reference image quality assessment in the spatial domain. *IEEE Transactions on Image Processing*, 21(12):4695–4708, 2012. doi: 10.1109/TIP.2012.2214050.
- Anish Mittal, Rajiv Soundararajan, and Alan C. Bovik. Making a “completely blind” image quality analyzer. *IEEE Signal Processing Letters*, 20(3):209–212, 2013. doi: 10.1109/LSP.2012.2227726.

- Long Ouyang, Jeff Wu, Xu Jiang, Diogo Almeida, Carroll L. Wainwright, Pamela Mishkin, Chong Zhang, Sandhini Agarwal, Katarina Slama, Alex Ray, John Schulman, Jacob Hilton, Fraser Kelton, Luke Miller, Maddie Simens, Amanda Askell, Peter Welinder, Paul Christiano, Jan Leike, and Ryan Lowe. Training language models to follow instructions with human feedback, 2022. URL <https://arxiv.org/abs/2203.02155>.
- Zhihong Shao, Peiyi Wang, Qihao Zhu, Runxin Xu, Junxiao Song, Xiao Bi, Haowei Zhang, Mingchuan Zhang, Y. K. Li, Y. Wu, and Daya Guo. Deepseekmath: Pushing the limits of mathematical reasoning in open language models, 2024. URL <https://arxiv.org/abs/2402.03300>.
- H.R. Sheikh and A.C. Bovik. Image information and visual quality. *IEEE Transactions on Image Processing*, 15(2):430–444, 2006. doi: 10.1109/TIP.2005.859378.
- Zeina Sinno and Alan Conrad Bovik. Large-scale study of perceptual video quality. *IEEE Transactions on Image Processing*, 28(2):612–627, 2019. doi: 10.1109/TIP.2018.2869673.
- Shaolin Su, Qingsen Yan, Yu Zhu, Cheng Zhang, Xin Ge, Jinqiu Sun, and Yanning Zhang. Blindly assess image quality in the wild guided by a self-adaptive hyper network. In *2020 IEEE/CVF Conference on Computer Vision and Pattern Recognition (CVPR)*, pp. 3664–3673, 2020. doi: 10.1109/CVPR42600.2020.00372.
- Wei Sun, Wen Wen, Xiongkuo Min, Long Lan, Guangtao Zhai, and Kede Ma. Analysis of video quality datasets via design of minimalistic video quality models, 2024. URL <https://arxiv.org/abs/2307.13981>.
- Hugo Touvron, Thibaut Lavril, Gautier Izacard, Xavier Martinet, Marie-Anne Lachaux, Timothée Lacroix, Baptiste Rozière, Naman Goyal, Eric Hambro, Faisal Azhar, Aurelien Rodriguez, Armand Joulin, Edouard Grave, and Guillaume Lample. Llama: Open and efficient foundation language models, 2023. URL <https://arxiv.org/abs/2302.13971>.
- Jing Wang, Haotian Fan, Xiaoxia Hou, Yitian Xu, Tao Li, Xuechao Lu, and Lean Fu. Mstrig: No reference image quality assessment based on swin transformer with multi-stage fusion, 2022. URL <https://arxiv.org/abs/2205.10101>.
- Yibin Wang, Zhimin Li, Yuhang Zang, Chunyu Wang, Qinglin Lu, Cheng Jin, and Jiaqi Wang. Unified multimodal chain-of-thought reward model through reinforcement fine-tuning, 2025a. URL <https://arxiv.org/abs/2505.03318>.
- Yibin Wang, Yuhang Zang, Hao Li, Cheng Jin, and Jiaqi Wang. Unified reward model for multimodal understanding and generation, 2025b. URL <https://arxiv.org/abs/2503.05236>.
- Yilin Wang, Sasi Inguva, and Balu Adsumilli. Youtube ugc dataset for video compression research. In *2019 IEEE 21st International Workshop on Multimedia Signal Processing (MMSP)*, pp. 1–5. IEEE, September 2019. doi: 10.1109/mmisp.2019.8901772. URL <http://dx.doi.org/10.1109/MMSP.2019.8901772>.
- Zhou Wang, A.C. Bovik, H.R. Sheikh, and E.P. Simoncelli. Image quality assessment: from error visibility to structural similarity. *IEEE Transactions on Image Processing*, 13(4):600–612, 2004. doi: 10.1109/TIP.2003.819861.
- Haoran Wei, Yaofeng Sun, and Yukun Li. Deepseek-ocr: Contexts optical compression, 2025. URL <https://arxiv.org/abs/2510.18234>.
- Haoning Wu, Chaofeng Chen, Jingwen Hou, Liang Liao, Annan Wang, Wenxiu Sun, Qiong Yan, and Weisi Lin. Fast-vqa: Efficient end-to-end video quality assessment with fragment sampling, 2022. URL <https://arxiv.org/abs/2207.02595>.
- Haoning Wu, Erli Zhang, Liang Liao, Chaofeng Chen, Jingwen Hou, Annan Wang, Wenxiu Sun, Qiong Yan, and Weisi Lin. Towards explainable in-the-wild video quality assessment: A database and a language-prompted approach. In *Proceedings of the 31st ACM International Conference on Multimedia, MM '23*, pp. 1045–1054. ACM, October 2023a. doi: 10.1145/3581783.3611737. URL <http://dx.doi.org/10.1145/3581783.3611737>.

- Haoning Wu, Zicheng Zhang, Weixia Zhang, Chaofeng Chen, Liang Liao, Chunyi Li, Yixuan Gao, Annan Wang, Erli Zhang, Wenxiu Sun, Qiong Yan, Xiongkuo Min, Guangtao Zhai, and Weisi Lin. Q-align: Teaching lmms for visual scoring via discrete text-defined levels, 2023b. URL <https://arxiv.org/abs/2312.17090>.
- Haoning Wu, Zicheng Zhang, Weixia Zhang, Chaofeng Chen, Liang Liao, Chunyi Li, Yixuan Gao, Annan Wang, Erli Zhang, Wenxiu Sun, Qiong Yan, Xiongkuo Min, Guangtao Zhai, and Weisi Lin. Q-align: Teaching lmms for visual scoring via discrete text-defined levels, 2023c. URL <https://arxiv.org/abs/2312.17090>.
- Haoning Wu, Hanwei Zhu, Zicheng Zhang, Erli Zhang, Chaofeng Chen, Liang Liao, Chunyi Li, Annan Wang, Wenxiu Sun, Qiong Yan, Xiaohong Liu, Guangtao Zhai, Shiqi Wang, and Weisi Lin. Towards open-ended visual quality comparison, 2024. URL <https://arxiv.org/abs/2402.16641>.
- Tianhe Wu, Jian Zou, Jie Liang, Lei Zhang, and Kede Ma. Visualquality-r1: Reasoning-induced image quality assessment via reinforcement learning to rank, 2025. URL <https://arxiv.org/abs/2505.14460>.
- Sidi Yang, Tianhe Wu, Shuwei Shi, Shanshan Lao, Yuan Gong, Mingdeng Cao, Jiahao Wang, and Yujiu Yang. Maniqa: Multi-dimension attention network for no-reference image quality assessment, 2022. URL <https://arxiv.org/abs/2204.08958>.
- Zhenqiang Ying, Haoran Niu, Praful Gupta, Dhruv Mahajan, Deepti Ghadiyaram, and Alan Bovik. From patches to pictures (paq-2-piq): Mapping the perceptual space of picture quality, 2019. URL <https://arxiv.org/abs/1912.10088>.
- Zhenqiang Ying, Maniratnam Mandal, Deepti Ghadiyaram, and Alan Bovik. Patch-vq: ‘patching up’ the video quality problem. In *2021 IEEE/CVF Conference on Computer Vision and Pattern Recognition (CVPR)*, pp. 14014–14024. IEEE, June 2021. doi: 10.1109/cvpr46437.2021.01380. URL <http://dx.doi.org/10.1109/CVPR46437.2021.01380>.
- Zhiyuan You, Xin Cai, Jinjin Gu, Tianfan Xue, and Chao Dong. Teaching large language models to regress accurate image quality scores using score distribution, 2025. URL <https://arxiv.org/abs/2501.11561>.
- Tianyu Yu, Haoye Zhang, Qiming Li, Qixin Xu, Yuan Yao, Da Chen, Xiaoman Lu, Ganqu Cui, Yunkai Dang, Taiwen He, Xiaocheng Feng, Jun Song, Bo Zheng, Zhiyuan Liu, Tat-Seng Chua, and Maosong Sun. Rlaif-v: Open-source ai feedback leads to super gpt-4v trustworthiness, 2024a. URL <https://arxiv.org/abs/2405.17220>.
- Zihao Yu, Fengbin Guan, Yiting Lu, Xin Li, and Zhibo Chen. Sf-iqa: Quality and similarity integration for ai generated image quality assessment. In *2024 IEEE/CVF Conference on Computer Vision and Pattern Recognition Workshops (CVPRW)*, pp. 6692–6701, 2024b. doi: 10.1109/CVPRW63382.2024.00663.
- Jingyi Zhang, Jiaying Huang, Huanjin Yao, Shunyu Liu, Xikun Zhang, Shijian Lu, and Dacheng Tao. R1-vl: Learning to reason with multimodal large language models via step-wise group relative policy optimization, 2025a. URL <https://arxiv.org/abs/2503.12937>.
- Lin Zhang, Lei Zhang, Xuanqin Mou, and David Zhang. Fsim: A feature similarity index for image quality assessment. *IEEE Transactions on Image Processing*, 20(8):2378–2386, 2011. doi: 10.1109/TIP.2011.2109730.
- Weixia Zhang, Kede Ma, Jia Yan, Dexiang Deng, and Zhou Wang. Blind image quality assessment using a deep bilinear convolutional neural network. *IEEE Transactions on Circuits and Systems for Video Technology*, 30(1):36–47, 2020. doi: 10.1109/TCSVT.2018.2886771.
- Weixia Zhang, Kede Ma, Guangtao Zhai, and Xiaokang Yang. Uncertainty-aware blind image quality assessment in the laboratory and wild. *IEEE Transactions on Image Processing*, 30: 3474–3486, 2021. ISSN 1941-0042. doi: 10.1109/tip.2021.3061932. URL <http://dx.doi.org/10.1109/TIP.2021.3061932>.

Weixia Zhang, Guangtao Zhai, Ying Wei, Xiaokang Yang, and Kede Ma. Blind image quality assessment via vision-language correspondence: A multitask learning perspective, 2023. URL <https://arxiv.org/abs/2303.14968>.

Xuanyu Zhang, Weiqi Li, Shijie Zhao, Junlin Li, Li Zhang, and Jian Zhang. Vq-insight: Teaching vlms for ai-generated video quality understanding via progressive visual reinforcement learning, 2025b. URL <https://arxiv.org/abs/2506.18564>.

Heliang Zheng, Huan Yang, Jianlong Fu, Zheng-Jun Zha, and Jiebo Luo. Learning conditional knowledge distillation for degraded-reference image quality assessment, 2021. URL <https://arxiv.org/abs/2108.07948>.

Hanwei Zhu, Haoning Wu, Yixuan Li, Zicheng Zhang, Baoliang Chen, Lingyu Zhu, Yuming Fang, Guangtao Zhai, Weisi Lin, and Shiqi Wang. Adaptive image quality assessment via teaching large multimodal model to compare, 2024. URL <https://arxiv.org/abs/2405.19298>.

## A COMPARED METHODS

1. **NIQE** Mittal et al. (2013): a handcrafted no-reference IQA model that assesses image quality by measuring deviations from natural scene statistics, without relying on any human-rated training data or prior knowledge of distortions.
2. **STEM** Kancharla & Channappayya (2022): a training-free method for assessing the quality of user-generated videos. Inspired by the human visual system’s perceptual straightening hypothesis, STEM measures how distortions increase the curvature of a video’s perceptual trajectory.
3. **BRISQUE** Mittal et al. (2012): a handcrafted NR-IQA model that evaluates image quality by measuring deviations from natural scene statistics of locally normalized luminance in the spatial domain, without requiring distortion-specific features or reference images.
4. **UNIQUE** Zhang et al. (2021): a deep learning–based BIQA model that learns to assess image quality through pairwise comparison and fidelity loss, enabling unified training across both synthetic and real-world distortions for robust generalization.
5. **MUSIQ** Ke et al. (2021): a deep learning–based IQA model that leverages a multi-scale Transformer architecture to assess image quality directly from images of arbitrary resolutions, capturing quality information at multiple granularities without the need for resizing or cropping.
6. **MANIQA** Yang et al. (2022): a deep learning–based NR-IQA model that employs a multi-dimensional attention architecture combining channel- and spatial-attention mechanisms (via Transposed Attention Block and Scale Swin Transformer Block) to jointly capture global and local visual dependencies, achieving superior performance—especially on GAN-distorted images.
7. **LIQE** Zhang et al. (2023): a MLMM-based BIQA method that leverages a multitask learning framework—jointly learning image quality, scene classification, and distortion identification—by aligning visual and textual embeddings through cosine similarity, enabling automatic parameter sharing and loss weighting for more robust and generalizable quality prediction.
8. **FAST-VQA** Wu et al. (2022): is an efficient deep video quality assessment framework that introduces a Grid Mini-patch Sampling strategy to retain both local and global quality information while drastically reducing computational cost. By processing these quality-preserving fragments through a specialized Fragment Attention Network, FAST-VQA enables effective end-to-end learning of video-quality-related representations.
9. **VQA<sup>2</sup>-Scorer** Jia et al. (2024): is a VQA model in the VQA2 series that leverages large multi-modal model architectures to predict quantitative quality scores for videos. It processes both spatial and temporal information by interleaving visual and motion tokens, enabling detailed perception of distortions and artifacts. Built upon the VQA2 Instruction Dataset, it is trained to capture nuanced quality differences across diverse video types, achieving strong performance in both traditional quality scoring and holistic visual quality understanding tasks.
10. **VQ-Insight** Zhang et al. (2025b): is a reasoning-driven MLLM framework designed for evaluating the quality of AI-generated videos (AIGC). It introduces a progressive video quality learning paradigm—starting from image-level warm-up, advancing to temporal understanding, and finally achieving joint optimization with video generators. Moreover, it incorporates multi-dimensional scoring, preference comparison, and temporal modeling rewards to balance generalization and specialization. Extensive experiments show that VQ-Insight outperforms state-of-the-art methods across multiple evaluation settings, offering reliable and interpretable video quality assessment for AIGC applications.
11. **VQThinker** Cao et al. (2025a): is a reasoning-based VQA framework that integrates LLMs with reinforcement learning to jointly perform video quality understanding and scoring, mimicking human perceptual judgment. It introduces a GRPO algorithm with three VQA-specific rewards—bell-shaped regression, pairwise ranking, and temporal consistency—to enhance quality reasoning and prediction accuracy. Experiments show that VQThinker achieves state-of-the-art performance, strong out-of-distribution generalization, and superior explainability in both quality scoring and distortion interpretation tasks.

12. **Q-Align** Wu et al. (2023c) : a MLLM-based method that trains LMMs for image and video quality assessment by emulating human raters’ use of discrete text-defined rating levels, enabling unified evaluation across IQA, IAA, and VQA tasks while achieving state-of-the-art performance.
13. **MinimalisticVQA** Sun et al. (2024): a ultra-simple blind video quality assessment model designed to analyze and benchmark VQA datasets. They are built using only basic components: a video preprocessor (for spatiotemporal downsampling), a spatial quality analyzer, an optional temporal quality analyzer, and a quality regressor, all implemented with the simplest possible methods. Despite their simplicity, MinimalisticVQA models reveal fundamental issues in existing VQA datasets, such as the easy dataset problem, and provide insights for designing more robust and generalizable BVQA models.
14. **DeQA-Score** You et al. (2025): a MLLM-based method that leverages MLLMs for precise image quality score regression by discretizing continuous score distributions into soft labels, preserving inter-image relationships, and employing a Thurstone-based fidelity loss to co-train across multiple IQA datasets, achieving stable performance aligned with human annotations.
15. **Q-Insight** Li et al. (2025): an MLLM-based approach that leverages reinforcement learning via GRPO to jointly optimize score regression and degradation perception, enabling visual reasoning for image quality understanding under limited supervision. However, its reward design primarily focuses on absolute score regression, which often leads to overfitting specific distributions and poor robustness when generalized to unseen datasets.
16. **VisualQuality-R1** Wu et al. (2025): an MLLM-based reasoning-driven no-reference image quality assessment model that employs reinforcement learning to rank for human-aligned, context-aware evaluation. Its pairwise ranking formulation emphasizes relative ordering without sufficient score calibration, resulting in score distributions that deviate from human perceptual preferences.
17. **Qwen2.5-VL-7B** Bai et al. (2025): is a pre-trained MLLM baseline used for comparison, providing strong multi-modal representation capabilities without task-specific fine-tuning.
18. **UnifiedReward-Think** Wang et al. (2025a): a unified multimodal reward model that extends UnifiedReward by incorporating explicit long CoT reasoning across both visual understanding and generation tasks. It employs a three-stage optimization process, including CoT reward initialization, rejection sampling-based generalization fine-tuning, and GRPO reinforcement refinement. By leveraging both explicit and implicit CoT reasoning, it achieves robust alignment with human perceptual judgments across diverse tasks.
19. **Our PreResQ-R1**: a Preference-Response Disentangled Reinforcement Learning framework for fine-grained and interpretable image quality assessment. It unifies absolute score regression and relative ranking consistency within a single reasoning-driven optimization paradigm. Specifically, PreResQ-R1 decomposes the reward into two complementary branches: a response-based component that enhances intra-sample coherence across multiple reasoning trajectories, and a preference-based component that preserves inter-sample perceptual ordering through magnitude-aware pairwise and triplet comparisons. Trained with GRPO and a two-stage Exploration-to-Stability fine-tuning strategy, PreResQ-R1 enables multimodal large language models to perform human-aligned, chain-of-thought reasoning about visual fidelity, achieving both high correlation accuracy and robust cross-domain generalization.

## B FURTHER METHODOLOGICAL INSIGHTS

**Why we decouple the video assessment into global-temporal dimension and local-spatial dimension.** Inspired by recent advances in DeepSeek-OCR, which compresses textual sequences into compact image tokens, we extend this idea to video quality assessment by representing temporal information at the image level. This motivates our decoupled design: the global-temporal branch captures overall motion consistency and smoothness by compressing multiple frames into a single global multiframe representation, as summarized in Fig. 8, enabling efficient reasoning over temporal coherence. In contrast, the local-spatial branch focuses on perceptual quality within individual

---

**Algorithm 1 PreResQ-R1: Two-stage fine-grained rank-and-score reinforcement learning for image quality assessment via preference–response disentangled policy optimization.**


---

**Input:** Training set  $\mathcal{D} = \{(\mathcal{I}_j, \mathcal{P}_j, \mathbf{G}_j)\}_{j=1}^B$ , pretrained policy  $\pi_\theta$ , reference policy  $\pi_{\text{ref}}$ , generation number  $K$ , batch size  $B$ , total steps  $T$ , reward weights  $\alpha, \beta_{\text{err}}, \beta_{\text{rank}}$ , and standard deviation penalty parameters  $\lambda_{\text{std}}, \Omega_{\text{std}}$ .

**Output:** Updated policy  $\pi_\theta$ .

- 1: **Stage 1: Multi-prompt Exploration with Std Penalty**
  - 2: **for** each image or video sample  $\mathcal{I}_i$  in dataset **do**
  - 3:     Randomly select a prompt  $\mathcal{P}_x$  from predefined set  $\{\mathcal{P}_I, \dots, \mathcal{P}_V\}$ .
  - 4:     Generate  $K$  responses  $\tau_j^{(1:K)} \sim \pi_\theta(\cdot | \mathcal{P}_x, \mathcal{I}_j)$ .
  - 5:     Extract dimension-wise scores  $\mathbf{s}_j^{(i)} = [s_j^1, \dots, s_j^5]$ .
  - 6:     Compute std penalty  $R_{\text{std}}(\mathbf{s}_j^{(i)})$  as Eq. (16).
  - 7:     Compute preference–response disentangled rewards  $R_{\text{for}}, R_{\text{loc}}^{j,i}, R_{\text{pair}}^{j,i}, R_{\text{tri}}^{j,i}, R_{\text{std}}$  (Eq. (2–9)).
  - 8:     Form total reward  $R_j^{(i)}$  as Eq. (10–11).
  - 9:     Update  $\pi_\theta$  via PRPO objective (Eq. (12–15)).
  - 10: **end for**
  - 11:  $\triangleright$  *Exploration RL2RS fine-tuning with PRPO optimization.*
  - 12: **Stage 2: Single-prompt Stability Refinement**
  - 13: **for** each image or video sample  $\mathcal{I}_i$  in dataset **do**
  - 14:     Use single standard prompt  $\mathcal{P}$  for generation.
  - 15:     Generate  $K$  responses  $\tau_j^{(1:K)} \sim \pi_\theta(\cdot | \mathcal{P}, \mathcal{I}_j)$ .
  - 16:     Extract predicted scores  $\mathbf{s}_j^{(i)}$ .
  - 17:     Compute rewards  $R_{\text{for}}, R_{\text{loc}}^{i,k}, R_{\text{pair}}^{i,k}, R_{\text{tri}}^{i,k}$  (Eq. (2–9)).
  - 18:     Obtain final reward  $R_j^{(i)}$  and normalize advantages  $a_j^{(i)}$  (Eq. (10–11)).
  - 19:     Update  $\pi_\theta$  via PRPO objective (Eq. (12–15)).
  - 20: **end for**
  - 21:  $\triangleright$  *Stability RL2RS fine-tuning with PRPO optimization.*
  - 22: **return** Optimized policy  $\pi_\theta$ .
- 

frames. Considering inference latency and computational efficiency, we randomly sample three key frames as representative inputs for local spatial evaluation. This design effectively balances global temporal perception with local spatial fidelity, leading to more robust and interpretable video quality assessment.

**Why we divide visual assessment into fine-grained details.** Human perception of visual quality is intrinsically multi-dimensional, encompassing interrelated factors such as texture fidelity, color saturation, contrast, and semantic clarity. Conventional IQA models that regress a single holistic score fail to capture these heterogeneous perceptual cues, leading to entangled representations and unstable reasoning. By decomposing assessment into five fine-grained perceptual dimensions (Saturation, Granularity, Sharpness, Foreground, and Background) PreResQ-R1 explicitly structures the visual reasoning process. This decomposition enforces a dimension-aware reasoning pathway that aligns linguistic explanations with visual evidence, thereby promoting fine-grained perceptual reasoning. The structured formulation further stabilizes optimization through dimension-wise regularization (e.g., standard deviation penalty) and reward balancing, ultimately enhancing interpretability, robustness, and perceptual fidelity.

**Why we introduce a preference–response disentangled policy optimization definition.** Conventional reward formulations in RL-based IQA reduce perceptual alignment to either scalar regression or ordinal ranking, neglecting the intertwined nature of intra-sample reasoning stability and inter-sample perceptual consistency that underpin human quality judgment. The proposed Preference–Response Disentangled Policy Optimization (PRPO) establishes a dual-axis reward geometry that decomposes optimization into response coherence and preference alignment. The former regularizes reasoning trajectories within each perceptual context, while the latter constrains global quality ordering across heterogeneous samples. This disentangled formulation transforms reward

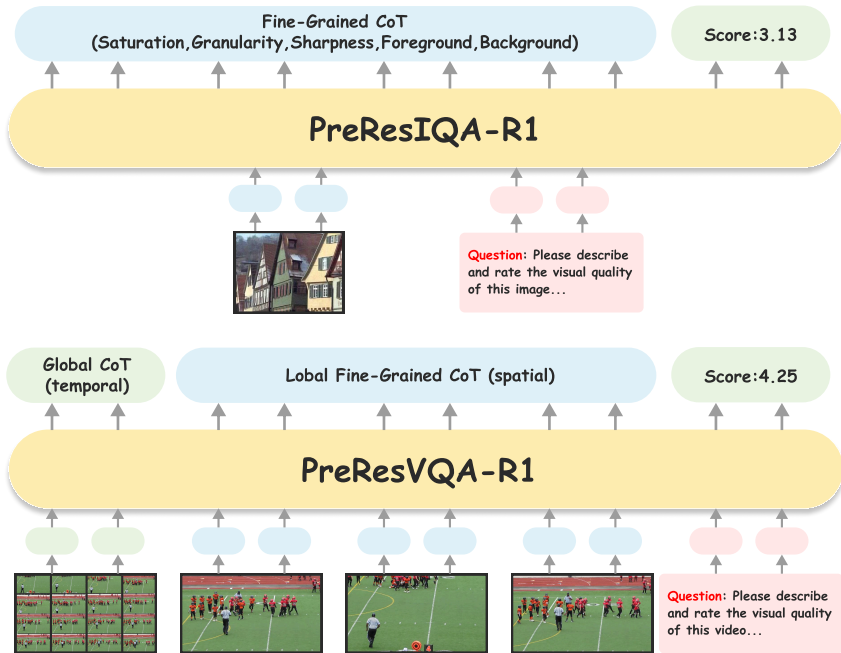


Figure 8: The input and output data flow in PreResIQA-R1 and PreResVQA-R1.

learning from distribution-specific scalar fitting into a structurally grounded perceptual reasoning process, preventing spurious reward exploitation and overfitting to dataset priors. By explicitly balancing local response fidelity and global perceptual regression, PRPO enforces reward discrimination, enhances policy robustness against distributional shift and reward hacking.

**Why we train only on KADID-6K dataset, and evaluate PreResQ-R1 on ten datasets.** Training solely on KADID-6K deliberately targets preference alignment rather than re-teaching visual perception: we assume the underlying MLLM already possesses strong visual understanding and reasoning priors, and **our goal is to use minimal RL fine-tuning to correct its deviations from human aesthetic preference**. This low-cost RL calibration nudges the model’s pre-trained perceptual priors toward human MOS with limited supervision. Evaluating across ten heterogeneous benchmarks—covering both synthetic and authentic distortions—provides a stringent out-of-distribution test: the consistently high SRCC and PLCC demonstrate that our disentangled PRPO framework effectively rectifies human–model preference bias while preserving the MLLM’s intrinsic generalization. In short, this work emphasizes efficient alignment (minimal RL intervention) over wholesale perceptual re-learning, offering a scalable path for human-aligned aesthetic assessment.

**Why we voluntarily introduce std penalty and response balance reward to obtain Exploration-to-Stability fine-tuning process.** We introduce a standard deviation penalty at the fine-grained answer level in first exploration stage to accelerate the model’s sensitivity to differences across granular aspects, enabling it to accurately predict each fine-grained component. The response balance reward promotes consistent and stable generations, which not only enhances overall training stability but also supports reliable preference ranking and score-based rewards. Together, these mechanisms ensure that the model learns nuanced distinctions while maintaining coherent and calibratable outputs.

**Why we introduce the preference triplet ranking score with the introduction of pairwise ranking and score reward.** While pairwise comparisons capture local perceptual consistency, they are insufficient to enforce global transitivity across multiple samples. The preference triplet ranking–score reward introduces a more challenging and fine-grained relational constraint by modeling third-order transitivity, guiding the policy to refine subtle perceptual distinctions and construct globally coherent hierarchies. By integrating pairwise and triplet consistency, we form a synergistic reward landscape—pairwise terms anchor local human alignment, whereas triplet terms eliminate cyclic inconsistencies and enhance global ranking stability.

**Multi-prompts in exploration-fine-tuning stage: why it works.** In the early exploration phase, fixed prompts tend to restrict reasoning diversity and confine the model’s attention to narrow perceptual patterns. Introducing multiple semantically varied prompts (e.g., focusing on “texture clarity,” “color naturalness,” or “composition balance”) stimulates broader Chain-of-Thought trajectories and exposes the model to different linguistic formulations of quality reasoning. This multi-prompt strategy acts as reward-level data augmentation, allowing the policy to explore a richer reasoning space and uncover diverse perceptual cues before convergence. Subsequent stability refinement distills this diversity into a calibrated policy, improving both reasoning coherence and generalization to unseen distortions.

## C PROMPTING TEMPLATES AND QUALITATIVE CASES

We provide a detailed overview of the overall algorithmic workflow in Algorithm 1, and present the complete prompt templates used for both IQA and VQA tasks in Table 4. To further complement our main results, we include extensive qualitative analyses and ablation studies in the supplementary figures. Specifically, Fig. 9, Fig. 11, and Fig. 10 illustrate additional comparison cases with state-of-the-art methods, as well as preference–response ablation analyses and step-wise training behaviors for the IQA task. Similarly, Fig. 12, Fig. 13, and Fig. 14 present corresponding results for the VQA task, offering a more comprehensive understanding of our model’s reasoning ability, robustness, and cross-domain generalization.

## D SOCIETAL IMPACTS

Our work presents PreResQ-R1, a reinforcement learning framework that advances the reasoning capability and interpretability of multimodal large language models in assessing perceptual visual quality. By unifying preference alignment and response consistency, this approach enhances the reliability of automated quality evaluation systems in domains such as photography, media compression, content generation, and visual communication. The societal benefit lies in promoting transparent, human-aligned assessments that can assist users, creators, and industries in maintaining high-quality visual standards while reducing subjective bias and annotation costs. However, the ability to model human-like reasoning about perceptual quality also entails potential risks. If deployed without proper safeguards, such systems may inadvertently reflect or amplify aesthetic or cultural biases inherent in the training data. Moreover, automated evaluation models could influence creative practices or decision-making processes in ways that prioritize algorithmic preferences over individual or cultural diversity. We therefore encourage responsible use of PreResQ-R1 and similar technologies, emphasizing fairness-aware data selection, transparent evaluation, and human-in-the-loop oversight when applied to subjective domains.

## E ETHICAL STATEMENT

This research adheres to recognized standards of academic integrity and ethical AI development. The study relies exclusively on publicly available datasets and does not involve any personally identifiable information, human subjects, or sensitive content. All experimental procedures, training protocols, and evaluations were designed to ensure transparency, reproducibility, and fairness. The objective of this work is to improve the interpretability and robustness of visual quality assessment, rather than to automate or replace human judgment in artistic or perceptual evaluation. To the best of our knowledge, this study raises no ethical concerns.

Table 4: Fine-grained structured text prompts for the visual quality assessment task.

<p><b>IQA Prompt 1</b></p> <p>You are doing an image quality assessment. Provide five ratings in the following order: saturation, granularity, sharpness, foreground, and background. Please rate 5 scores. Each rating should be a float between 1 and 5, rounded to two decimals (1 = very poor, 5 = excellent).</p>
<p><b>IQA Prompt 2</b></p> <p>You are doing an image quality assessment. For this image quality assessment task, please evaluate along five aspects: color saturation, texture granularity, clarity or sharpness, foreground quality, and background quality. Please rate 5 scores each row. Give each aspect a score between 1.00 and 5.00 (two decimals, where 1 = very poor and 5 = excellent).</p>
<p><b>IQA Prompt 3</b></p> <p>You are doing an image quality assessment. Please assess image quality by providing five ratings in sequence: rate the saturation, rate the granularity, rate the sharpness, rate the foreground quality, and rate the background quality. Please rate 5 scores. All answers must be floats from 1.00 to 5.00, rounded to two decimals.</p>
<p><b>IQA Prompt 4</b></p> <p>You are doing an image quality assessment. Provide ratings for five dimensions: saturation to reflect color vividness, granularity to capture texture smoothness, sharpness to evaluate detail clarity, foreground quality to assess object visibility, and background quality to measure scene consistency. Please rate 5 scores each row. Each score must be a float between 1.00 and 5.00, where 1 means poor and 5 means excellent.</p>
<p><b>IQA Prompt 5</b></p> <p>You are doing an image quality assessment. Please give an image quality evaluation with five scores in the following order: saturation, granularity, sharpness, foreground quality, and background quality. Please rate 5 scores each row. Each score should be a float between 1 and 5, rounded to two decimals, with 1 indicating very poor quality and 5 indicating excellent quality.</p>
<p><b>IQA Template</b></p> <p>You are doing the image quality assessment task. Please describe and rate the picture in five parts: saturation rating; granularity rating; sharpness rating; foreground rating; and background rating. All ratings should be floats between 1 and 5, rounded to two decimals, where 1 represents very poor quality and 5 represents excellent quality.</p> <p>&lt;think&gt; ...Reasoning CoT... &lt;/think&gt; &lt;answer&gt;Score1; Score2; Score3; Score4; Score5&lt;/answer&gt;</p>
<p><b>VQA Template</b></p> <p>You are doing the video quality assessment task. Please compare the internal packed video frames in the first picture and describe the global multiframe pictures in temporal deminsion and global scene. Then compare and describe the rest local single frame pictures in five parts: saturation rating; granularity rating; sharpness rating; foreground rating; and background rating. Finally, please rate two scores in the global multiframe and local single frame dimension. All ratings should be floats between 1 and 5, where 1 represents very poor quality and 5 represents excellent quality.</p> <p>&lt;think&gt; ...Reasoning CoT... &lt;/think&gt; &lt;answer&gt;Score1; Score2&lt;/answer&gt;</p>

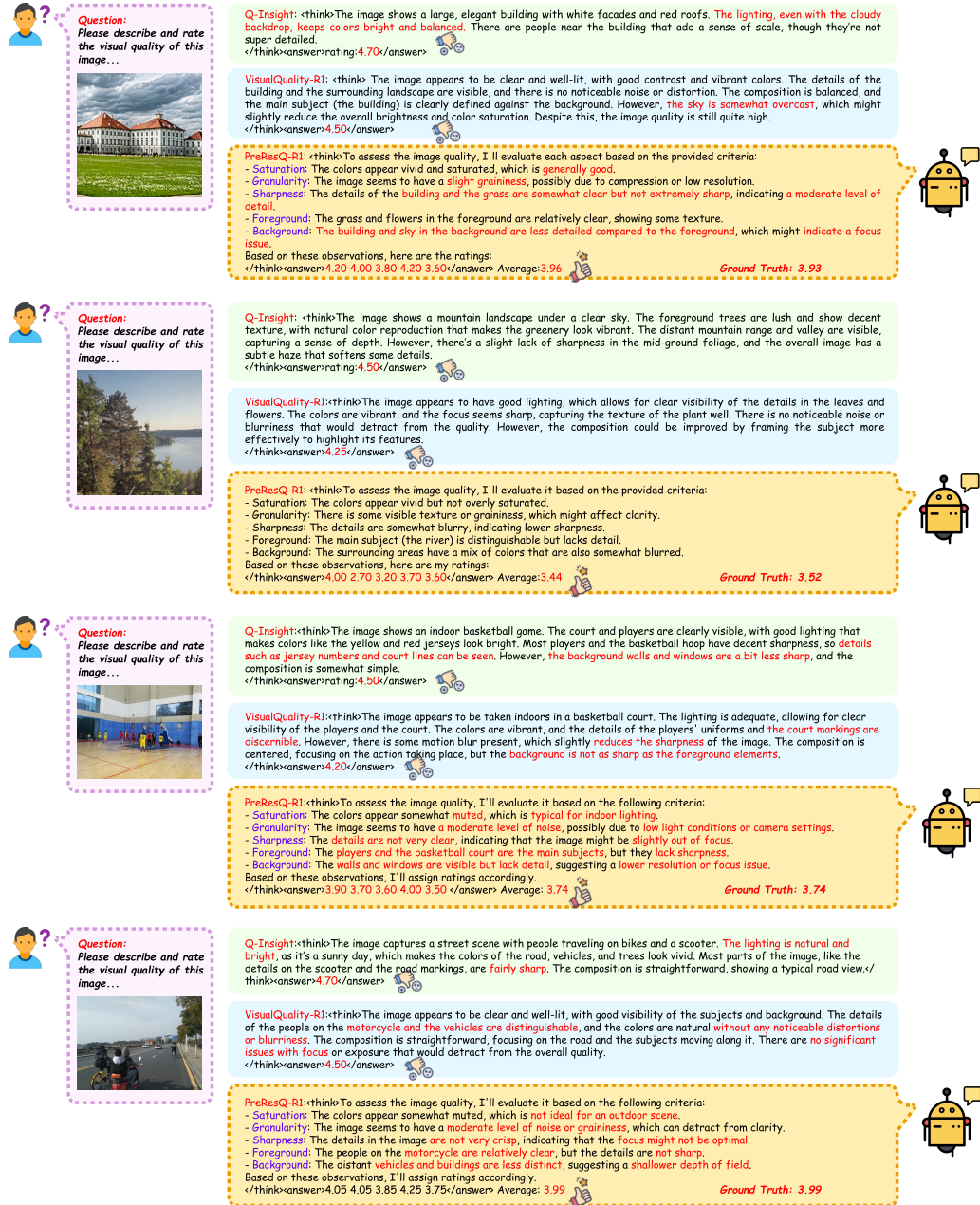


Figure 9: Qualitative comparison cases of image quality assessment results between PreResQ-R1 and state-of-the-art reinforcement learning based reasoning MLLM. Given an image, and a text prompt, our model performs quality assessment across saturation, granularity, sharpness, foreground, and background through CoT reasoning.

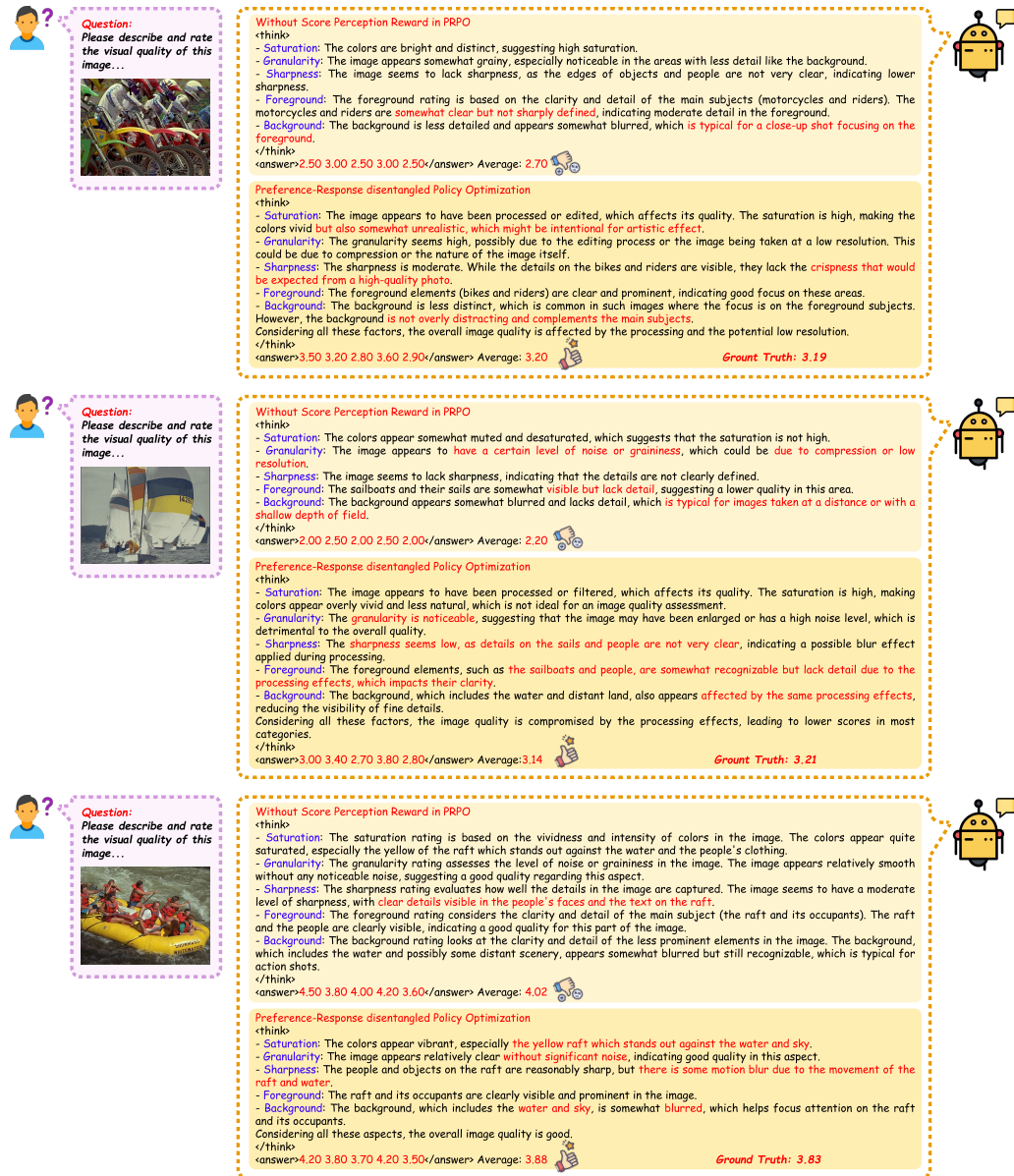


Figure 10: Qualitative ablation cases of PreResQ-R1's image quality assessment results with/without Score Perception Reward in Preference-Response disentangled Policy Optimization.

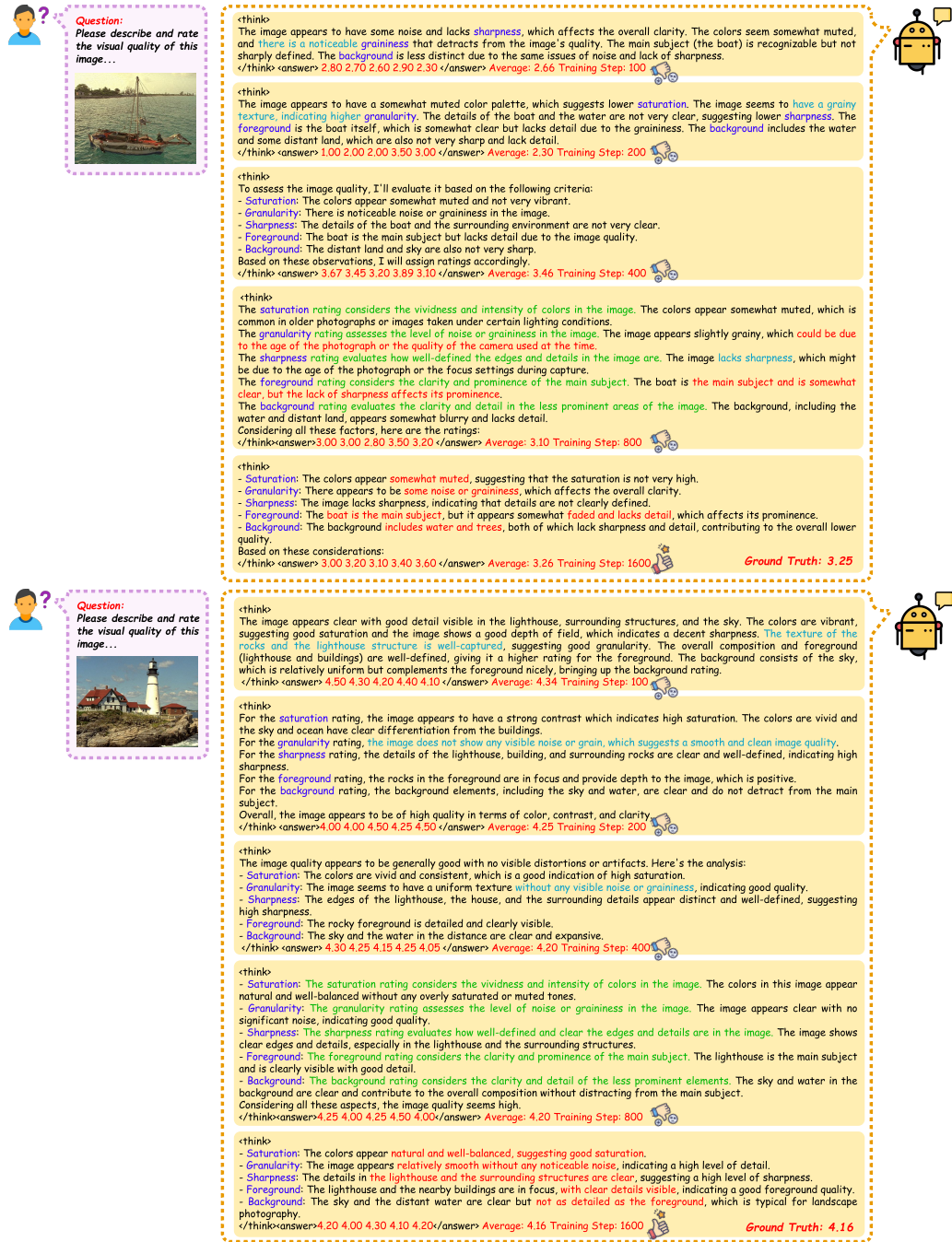


Figure 11: Qualitative comparison cases of PreResQ-R1's image quality assessment results across different training steps.

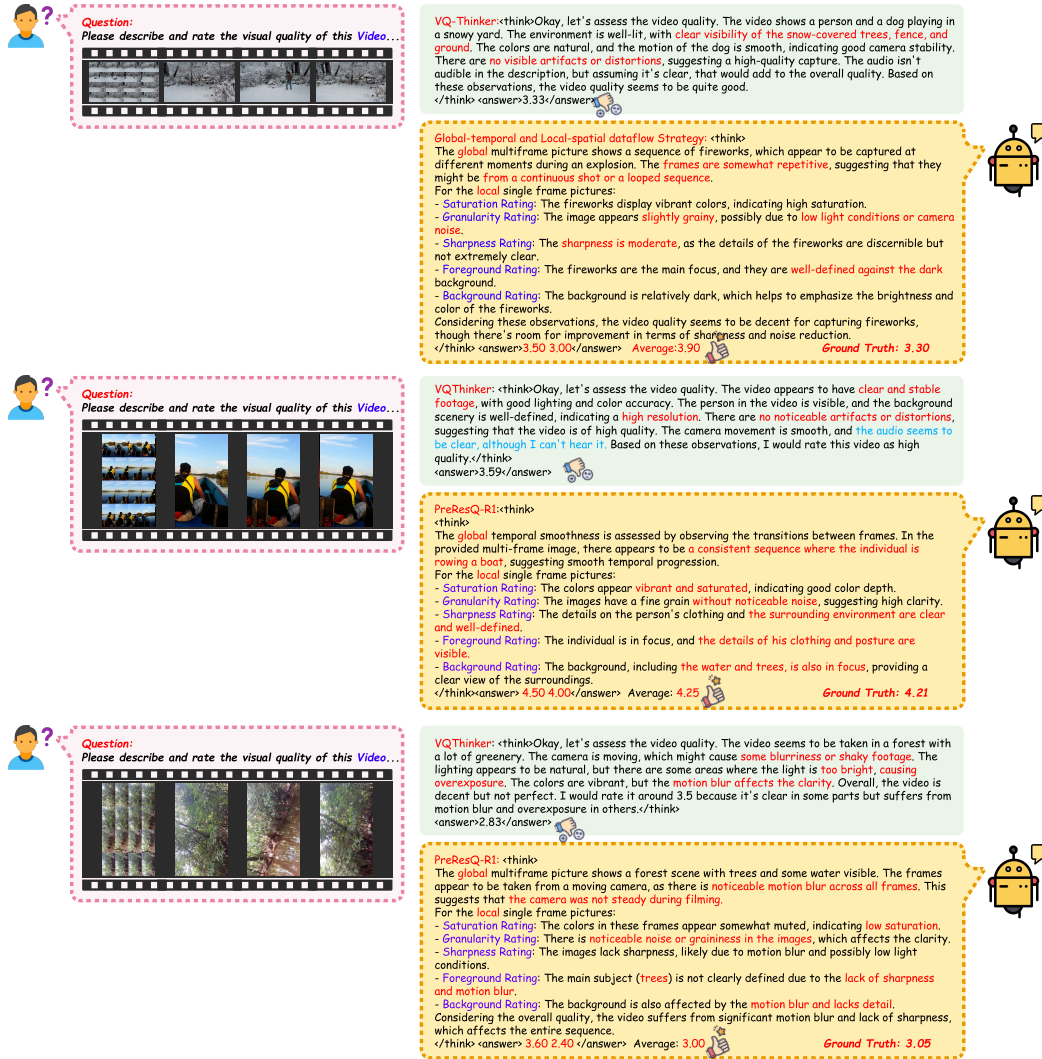


Figure 12: Qualitative comparison cases of video quality assessment results between PreResQ-R1 and state-of-the-art reinforcement learning based reasoning MLLM. Given an video sample, and a text prompt, our model performs quality assessment across saturation, granularity, sharpness, foreground, and background through CoT reasoning.

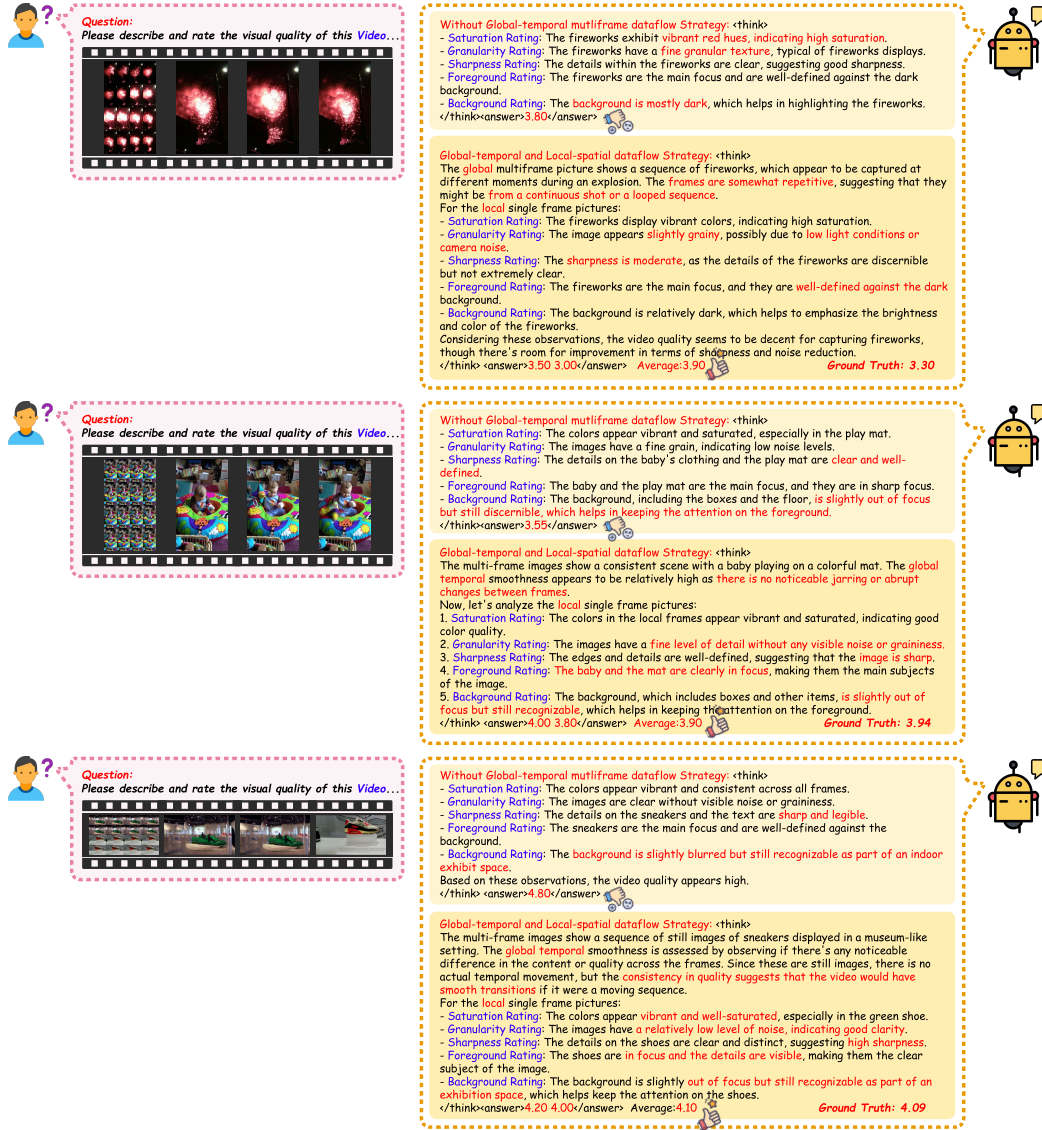


Figure 13: Qualitative ablation cases of PreResQ-R1's video quality assessment results with/without Global-Temporal dimension CoT in reasoning process.



Figure 14: Qualitative comparison cases of PreResQ-R1's video quality assessment results across different training steps.